Four core properties of the human brain valuation system demonstrated in intracranial signals

Alizée Lopez-Persem, Julien Bastin, Mathilde Petton, Raphaëlle Abitbol, Katia Lehongre, Claude Adam, Vincent Navarro, Sylvain Rheims, Philippe Kahane, Philippe Domenech, et al.

Four core properties of the human brain valuation system demonstrated in intracranial signals

Author List and affiliations

Alizée Lopez-Persem*[1,2], Julien Bastin[3], Mathilde Petton[4,5], Raphaëlle Abitbol[1,2], Katia Lehongre[2], Claude Adam[2,6], Vincent Navarro[2,6], Sylvain Rheims[4,5,7], Philippe Kahane[3,8], Philippe Domenech[2,9,10,11], Mathias Pessiglione*[1,2]

(1) Motivation, Brain and Behavior team, Institut du Cerveau (ICM), Paris, France
(2) ICM, INSERM UMRS 1127, CNRS UMR 7225, Sorbonne Université, Paris, France
(3) Grenoble Institut Neuroscience (GIN), INSERM U1216, University of Grenoble Alpes, Grenoble, France
(4) Lyon Neuroscience Research Center, INSERM U1028, CNRS UMR5292, Lyon-Bron, France
(5) Université Claude Bernard Lyon 1, France
(6) AP-HP, Epilepsy Unit, INSERM U1028, CNRS UMR5292, Paris, France
(7) Department of Functional Neurology and Epileptology, Hospices Civils de Lyon and Lyon 1 University, Lyon, France
(8) CHU Grenoble Alpes, Grenoble, France
(9) Neurophysiology of Repetitive Behavior team, Institut du Cerveau (ICM), Paris, France
(10) Université Paris-Est Créteil, Créteil, France.
(11) CHU Henri Mondor, DMU Psychiatrie et d'Addictologie, Créteil, France

* Corresponding authors: lopez.alizee@gmail.com and mathias.pessiglione@gmail.com

Abstract

Estimating the value of alternative options is a key process in decision-making. Human fMRI and monkey electrophysiology studies have identified brain regions composing a valuation system, such as the ventromedial prefrontal and lateral orbitofrontal cortex (vmPFC and lOFC). Here, in an effort to bridge across species and techniques, we investigated the neural representation of value ratings in 36 human patients, using intracranial electroencephalography. We found that subjective value was positively reflected in both vmPFC and lOFC high-frequency activity, plus several other brain regions, including the hippocampus. We then demonstrated that subjective value could be decoded (1) in pre-stimulus activity, (2) for various categories of items, (3) even during a distractive task and (4) as both linear and quadratic signals (encoding both value and confidence). Thus, our findings specify key functional properties of neural value signals (anticipation, generality, automaticity, quadraticity), which might provide insights into human irrational choice behaviors.

Brief summary

Lopez-Persem et al. used intracranial recordings in human patients to uncover key functional properties of neural value signals that might explain irrational choice behavior.

Introduction

Standard decision-making theory assumes that making a choice involves two steps: first estimating the value of alternative options and then comparing these values to select the best option. While neural and computational models have been suggested for the value comparison process[1,2], the value estimation process remains poorly understood[3,4]. Subjective values can be inferred from choice tasks, when several options are available, or elicited more directly using judgement tasks, when a single option is rated on a likeability scale[5].

In the last decade, numerous studies, using either choice or rating tasks, have concurred to delineate a set of brain regions reflecting subjective values, termed brain valuation system (BVS)[6]. Meta-analysis of fMRI studies in humans have designated the ventromedial prefrontal cortex (vmPFC), the ventral striatum (vS) and the posterior cingulate cortex (pCC) as key components of the BVS[7,8]. However, many other brain regions have been reported to signal subjective values in particular fMRI studies. For instance, the hippocampus might critically

contribute to valuation when it involves imagining what the outcome would be like[8,9]. This is in accordance with the well-established notion that the hippocampal cortex (HC) can provide information stored in memory when a hypothetical episode needs to be assembled[10,11]. Also, the lateral part of the orbitofrontal cortex (lOFC) has been implicated in cue-outcome association paradigms involving reward and punishment[12,13]. Interestingly, other approaches such as intracranial single-cell recordings in monkeys have identified neurons reflecting subjective values not only in the vmPFC[14,15], but also in many other brain regions, notably the lOFC[16,17]. Consistently, a recent study using electrocortigraphy (ECoG) electrodes placed on the cortical surface have described reward-related activity in the human lOFC during a gambling task[18].

In an effort to bridge across techniques and species, we investigated the human brain with intracranial electro-encephalography (iEEG), which gives access to local field potentials in deep structures of the human brain. Thus, iEEG recordings avoid the attenuation and spatial diffusion of electric signals that are collected with scalp electrodes. Also, contrary to hemodynamic signals recorded with fMRI, they offer much better temporal resolution (milliseconds instead of seconds). Such recordings can be obtained in patients with drug-resistant focal epilepsy, who are implanted with intracranial electrodes for up to two weeks before surgery. This period provides a unique window into iEEG dynamics during performance of cognitive tasks in humans.

A first aim of our study was to identify which brain regions and which frequency bands were involved in generating value signals detectable with deep electrophysiology in humans. Contrary to typical electrophysiology studies, we did not select a priori the regions where electrodes were implanted, and collected data from 4273 recording sites, disseminated throughout the brains of 36 patients. A second aim was to compare the functional properties of these value signals with those previously described in fMRI studies. We focused on four core properties, which can be elicited with judgment tasks. These tasks, virtually impossible to implement in monkeys, have the advantage of presenting one item per trial, which facilitates tracking of value representations in brain activity, compared to choice tasks presenting two options or more.

All four functional properties have been identified from fMRI signals recorded in the vmPFC, and occasionally found in other BVS regions such as the vS, HC and pCC. First, the value signal recorded in the BVS depends on pre-stimulus baseline activity, which itself depends on the pleasantness of the internal or external context (e.g., mood level or background music)[19,20].

Second, the BVS can assign values to different categories of objects, such as food, money, trinkets, faces, paintings, houses, charities etc.[21,22], in accordance with the idea of a common neural currency[23]. Third, the BVS expresses subjective value in an automatic manner, meaning even if subjects are engaged in a distractive task[22], or passively viewing choice options[24]. Fourth, the BVS not only reflects option or decision value, but also confidence in the judgment or choice[25,26].

These properties are important because, taken together, they might explain some irrational judgements, such as the well-known misattribution bias (when distractors affect the value of target features) or the desirability bias (when expected value affects confidence). Indeed, these biases might arise from interference or spill-over effects, due to the fact that value and confidence relating to various features are automatically represented in the same neural substrates, whose activity may affect subsequent judgement or choice.

In order to assess the functional properties of value representation, we used different categories of items (food, faces, paintings), value-based and non-value-based first-order judgments (likeability and age ratings), and second-order judgments (confidence ratings). We first identified value signals across brain regions and frequency domains. Then we focused on regions of interest (ROI), not only those typically found in meta-analyses of fMRI studies (such as the vmPFC), but also others (such as the lOFC and HC) that together constitute the BVS. In each of these ROI, we tested whether the value signal would be anticipatory (predicting likeability rating in a pre-stimulus time window), generic (signaling the values of both food and non-food items), automatic (signaling value during the age rating task) and quadratic (reflecting confidence across first-order ratings).

Results

Behavior: linking value to choice, confidence and response time

36 patients suffering from epilepsy (37.9 ± 10.7 years old, 21 females, see demographical details in Supplementary Table 1) performed a series of rating and choice tasks (Figure 1a-c). One subset of patients (n=22) performed a short version of the behavioral tasks that only contained food items. In a first block, they had to rate the likeability of all food items presented one by one. In a second block, they had to choose between items of the same pool, now presented in pairs, according to their subjective preference. The other subset of patients (n=14) performed a long version of the same behavioral tasks, which added three components. First,

two other categories of items were included (faces and paintings) to assess the generality of value signaling. Second, a distractive task, in which patients rated the age of faces and paintings, was inserted to assess the automaticity of value signaling. Third, a confidence rating task was added on top of age and likeability ratings, in order to test the quadratic link between the two levels (first-order and second-order) of ratings. The two additional categories (face and painting) were also inserted in the choice task to check the relationship between likeability rating and pairwise preference. Trials were blocked such that all choices were made between items from the same category. Note that the age rating task was always performed first in these patients, to avoid priming valuation processes with the likeability rating task. The choice task was always performed last, so the pairing of items could be adjusted on the basis of their likeability ratings (see methods). The distributions of ratings and response times are provided in Extended Data 1 and 2.

We first tested whether subjective values could predict rating confidence and RT (Figure 1d-e), in the subset of patients who performed the long version of the task (black dots), pooling non-food items (faces and paintings) to increase statistical power. Using individual-level polynomial regression followed by group-level two-sided t-tests on regression coefficients, we confirmed a quadratic (U-shaped) relationship between first-order (age and likeability) and second-order (confidence) ratings (β_{quad}=0.21±0.03, t(13)=6.36, p=2.10^{-5}). This quadratic link was significant for both food and non-food items and for both age and likeability rating tasks ($\beta_{quad/non-food/age}$=0.16±0.04, t(13)=4.62, p=5.10^{-4}; $\beta_{quad/non-food/like}$=0.30±0.06, t(13)=4.92, p=3.10^{-4}; $\beta_{quad/food/like}$=0.38±0.08, t(13)=4.79, p=4.10^{-4}). Note that a linear term was included in the polynomial fit, but was only significant for confidence in age rating ($\beta_{lin/non-food/age}$=-0.14±0.05, t(13)=-2.81, p=0.01), probably reflecting the fact that some ages were easier to rate than others.

We also observed a significant quadratic link (inverted U-shape, β_{quad}=-0.30±0.06, t(13)=-4.96, p=2.10^{-4}) between first-order rating and rating RT (from item display to first button press). This quadratic link was significant for both types of items and for both types of judgments ($\beta_{quad/non-food/age}$=-0.48±0.02, t(13)=-2.53, p=0.025; $\beta_{quad/non-food/like}$=-0.34±0.09, t(13)=-3.66, p=3.10^{-3}; $\beta_{quad/food/like}$=-0.33±0.01, t(13)=-2.93, p=0.012). The linear term included in the polynomial fit was not significant (all p>0.17). We also tested the possibility of higher-order effects by including a cubic term in the polynomial regressor. Results were unchanged for the linear and quadratic terms, with the cubic term being non-significant in every case (all p>0.05).

Next, we tested whether subjective values could predict preferences recorded in the choice task (Figure 1f), starting with behavioral data obtained from the short version (including food items

only) that was common to all 36 patients (red dots). Individual logistic regression of choice rate (in a left versus right frame) against decision value (left minus right item likeability rating) showed a significant link at the group level (β_{Food}=0.42±0.07, t(34)=6.4, p=2.10^{-7}). Linear regression of choice response time (RT) against unsigned decision value, which is taken as an inverse proxy for choice difficulty, was also significant (β_{Food}=-72.8±14.0, t(34)=-5.19, p=9.10^{-6}). We then applied the same regression analyses to data from tasks that were specific to the long version (black dots). Again, we found that signed decision value predicted choice rate ($\beta_{Non\text{-}Food}$=-125±0.03, t(13)=12.8, p=6.10^{-8}) and that unsigned decision value predicted choice RT ($\beta_{Non\text{-}Food}$=0.37±19.8, t(13)=-6.32, p=6.10^{-5}). When these analyses were applied to face and painting separately, the results were also significant (choice rate: β_{Face}=0.38±0.05, t(12)=7.34, p=1.10^{-5}, $\beta_{Painting}$=0.48±0.10, t(13)=4.68, p=4.10^{-4}; choice RT: β_{Face}==-121±22.2, t(12)=-5.43, p=2.10^{-4}, $\beta_{Painting}$==-113±22.2, t(13)=-5.09, p=2.10^{-4}) and no significant difference was observed between regression estimates when comparing the three categories of items two by two (all p>0.05). We also verified that decision value was a significant predictor of choice in every individual patient for all three categories (all p<0.05).

Altogether, they confirmed that likeability ratings provide reliable estimates of subjective value, being significant predictors of various behavioral measures such as choice, response time and confidence (see Figure 1d-f). In the following, we focus on brain activity recorded during the rating tasks (Figure 1a and 1b), in which only one visual item was on screen at a time, making it possible to isolate the neural correlates of its subjective value.

Intracranial EEG: localizing value signals, a pseudo whole-brain analysis

Among our 4273 contacts distributed over the 36 patients, we could analyze 3194 good-quality bipolar signals, located in 77 regions of the AAL atlas[27], each with at least 9 recording sites (Figure 2, Supplementary Table 2). For this pseudo whole-brain analysis, we focused on high-gamma band activity (in the 50-150Hz a priori range), since it is assumed to provide a bridge between fMRI[28,29] and spiking activity[30,31]. High-gamma power was extracted from every recording site time-series and regressed at each time point against subjective value. We took likeability rating obtained for food items as the main proxy for subjective value, because it was collected in all our patients. For each brain region of the restructured AAL atlas, we tested the significance of regression estimates in a fixed-effect analysis (pooling sites across patients) with correction for multiple comparisons across time points through non-parametric cluster-level

194 statistics (see methods).
195 In the high-gamma frequency band, we found 18 ROIs (over 77 analyzed ROIs) showing a
196 significant expression of subjective value, after correcting for multiple comparisons across
197 ROIs, with more than 20% of significant recording sites (Supplementary Table 3). This set of
198 significant ROIs included the medial, middle and superior orbitofrontal cortex (vmPFC and
199 lOFC), bilaterally. Among other significant brain regions, we retained those showing strong
200 bilateral value signaling: the hippocampus and para-hippocampal cortex (PHC), the anterior
201 cingulate gyrus, the anterior fusiform area, the inferior temporal cortex and the inferior frontal
202 opercularis.
203 In the main results reported below, we focus on the a priori regions of interest, namely the
204 vmPFC, lOFC, hippocampus and PHC (see anatomical locations in Figure 3a, Extended Data
205 3 and 4). These four regions are referred to as the BVS and analyzed as two sub-systems, the
206 OFC (including vmPFC and lOFC) and the (P)HC (including hippocampal and para-
207 hippocampal cortex). We checked that the recording sites in these four main ROIs were
208 similarly distributed across patients (Extended Data 3). The other regions expressing significant
209 value signals are analyzed in the same way, and the results are presented as Extended Data.
210 Together, they form what we hereafter call 'the extended BVS' (highlighted in Supplementary
211 Table 3).
212

213 **Investigation of value signals across ROIs and frequency bands**

214 In each ROI, we explored the other frequency bands to assess whether our prior on the
215 high-gamma band was justified. We first performed a time-frequency analysis on the evoked
216 response (time-locked on item onset), averaged across all sites in a given ROI (Figure 3b). The
217 time-frequency pattern was similar between vmPFC and lOFC on the one hand, and between
218 HC and PHC on the other hand. We noticed that in the OFC, the border between increase in
219 high-gamma power and decrease in gamma power was around 70Hz, so we refined our prior
220 on the high-gamma band (from 50-150 to 70-150Hz). We also checked that anatomical
221 boundaries between vmPFC and lOFC were correctly positioned, by tracking value signals
222 along the medio-lateral axis. The strongest value signals were indeed found around the center
223 of each ROI (Extended Data 4).
224 In order to define a time-window of interest for the following analyses, we extracted the
225 regression estimates of the vmPFC, lOFC, hippocampus and PHC from the pseudo-whole brain
226 analysis, for each time point between -0.2 and 1.5s around item onset (Figure 3d). We observed

a significant association (cluster-corrected, see methods) in the 0.77-1.03s window for the vmPFC, 0.36-1.00s for the lOFC, 0.16-1.28s for the hippocampus and 0.39-0.94s for the PHC. Examination of time courses suggests that value signals emerged later in the vmPFC compared to other ROIs. To better specify the propagation of value signals, we conducted cross-correlation analyses (see supplementary information). In the following analyses (Figure 3c), we focus on the 0.5-1s post-stimulus time window, which approximately corresponds to increased regression estimates in the four ROIs, hence to the valuation stage.

We found significant value signal for the four ROI in both gamma (vmPFC: β=0.044±0.0076, $t(72)$=5.78, $p=2.10^{-7}$; lOFC: β=0.037±0.0063, $t(151)$=5.57, $p=1.10^{-7}$; HC: β=0.0299±0.0058, $t(139)$=5.11, $p=1.10^{-6}$; PHC: β=0.036±0.011, $t(60)$=3.46, $p=9.10^{-4}$; two-sided one-sample t-tests) and high-gamma band (vmPFC: β=0.029±0.010, $t(72)$=2.89 $p=5.10^{-3}$; lOFC: β=0.046±0.0075, $t(151)$=6.09, $p=8.10^{-9}$; hippocampus: β=0.051±0.0073, $t(139)$=6.94, $p=1.10^{-10}$; PHC: β=0.0289±0.011, $t(60)$=2.59, p=0.012). However, there was a significant divide between these two high-frequency and the lower-frequency bands, in every ROI (vmPFC: $t(72)$=3.99, $p=2.10^{-4}$; lOFC: $t(151)$=6.26, $p=4.10^{-9}$; HC: $t(139)$=6.13, $p=8.10^{-9}$; PHC: $t(60)$=4.07, $p=1.10^{-4}$; two-sided one-sample paired t-tests).

To compare the contribution of the different frequency bands to value signals in the BVS (pooling the 4 ROIs), we regressed food likeability ratings against power in all frequency bands as separate regressors. The contribution of high-frequency bands were about 10 times that of lower frequency bands ($\beta_{H\gamma}$=0.254±0.032, β_{γ}=0.122±0.015, β_{β}=0.026±0.011, β_{α}=-0.06±0.016, β_{θ}=-0.011±0.012). To further check that low-frequency bands were not adding any information about subjective value, we compared GLMs including only high-gamma and gamma bands to all possible GLMs containing these high-frequency bands plus any combination of low-frequency bands. Bayesian model selection (see Methods) designated the high-frequency GLM as providing the best account of subjective value (Ef=0.83, Xp=1).

Thus, even if low-frequency activity was significantly related to subjective value, it carried redundant information relative to that extracted from high-frequency activity. Consequently, we only kept gamma and high-gamma bands (grouped into the 'high-frequency' range) for the investigation of functional properties. The ROI analysis just extends the expression of subjective value to the gamma band, and circumscribes its temporal occurrence (around 0.5-1s post-stimulus).

The same time-frequency investigation was conducted in supplementary ROIs composing the extended BVS (Extended Data 5). Although value signals were weaker in these regions, they

shared similar features. The regression of food likeability ratings against high-gamma activity revealed significant clusters in the 0.5-1s time window for all regions. In addition, significant positive links were only observed in gamma and high-gamma bands, and negative links in the theta and alpha bands. This pattern was globally true at the (pseudo) whole-brain level: positive associations with value were mostly observed in high-frequency bands and negative associations in low-frequency bands (Supplementary Tables 3-7).

Testing the core properties of value coding in the Brain Valuation System

In the following analyses, we tested whether the core properties of the BVS identified with fMRI (anticipation, generality, automaticity, quadratic coding) are also observable in iEEG activity. Note that all these tests are independent from the selection of anatomical ROI, which was based on the linear regression of post-stimulus time-series against food likeability ratings. Thus, we extended regression analyses to other time windows (pre-stimulus or pre-response), other categories (non-food items), other type of judgement (age rating) and other type of coding (quadratic).

Anticipation (baseline activity predicts value judgments)

For this analysis, we included a pre-stimulus time window (-0.2-0s), in addition to the pre-defined post-stimulus time window (0.5-1s). As expected, the association with food likeability rating (Figure 4) was significant in the post-stimulus time window for both ROIs (OFC: $t(449)=10.28$, $p<10^{-22}$, (P)HC: $t(401)=9.46$, $p=2.73.10^{-19}$; two-sided one-sample t-tests). In the pre-stimulus time window, regression estimates were significant in the OFC ($t(449)=2.38$, $p=0.018$), but not in the (P)HC ($t(401)=-1.57$, $p=0.12$). We noted that anticipatory value signaling was not observed when restricting the dataset to patients performing the long version of the task, but this is likely due to the reduction in statistical power.

Nevertheless, anticipatory value signaling was confirmed by a decoding analysis in which a classifier was trained to decode high versus low ratings (see methods and Extended Data 6). In the OFC, two time-windows showed significant decoding (pre-stimulus: from -0.192 to 0.032s, $p_{corr}=0.01$ and post-stimulus: from 0.352 to 1.104s, $p_{corr}<0.01$), while in the (P)HC, only one time window showed significant decoding (post-stimulus: from 0.480 to 0.992s, $p_{corr}<0.01$).

In order to better understand this effect, we conducted a tertian-split analysis of the raw high-frequency activity recorded in each ROI. Activity recorded between -0.2 and 1.5s was averaged separately for high and low rating trials, in each patient and ROI (Extended Data 7). The shift in pre-stimulus activity was mostly observed in the vmPFC, for likeability ratings (not age

ratings). As previously observed with fMRI[19], the raw signal change was a post-stimulus decrease, which was less pronounced for high values. Interestingly, the temporal dynamics of the signal was somewhat different between high and low rating trials, with faster changes for high values, which could explain why the time-locked correlation with value was lost between 0 and 0.4s after stimulus onset.

Generality (evoked activity reflects value judgments for different categories of items)

To investigate whether the BVS would signal subjective value across categories, we extended the linear regression to the likeability of non-food items, which were obtained in the subset of patients who performed the long version of behavioral tasks.

First, we checked whether the likeability of food items was represented in the electrodes of this subset of patients (63 and 73 recording sites in the OFC and (P)HC respectively), in the same time window (0.5-1s post-stimulus). We found significant regression estimates in each ROI (OFC: $t(125)=4.25$, $p=4.10^{-5}$, (P)HC: $t(145)=5.17$, $p=8.10^{-7}$; two-sided one-sample t-tests). Thus, regression against food likeability rating gave similar results (Figure 5a) as observed in the whole dataset (225 and 201 recording sites in the OFC and (P)HC respectively).

Then, we conducted the same regression analysis against the likeability of non-food items (Figure 5b). We found significant regression estimates for each ROI (OFC: $t(125)=2.62$, $p=0.01$, (P)HC: $t(145)=2.34$, $p=0.02$; two-sided one-sample t-tests), confirming that they were signaling the value of items from different categories.

Automaticity (evoked activity reflects value judgments during non value-related tasks)

To assess whether the BVS would also reflect subjective value during a distractive task, we extended the linear regression against the likeability of non-food items to the power time-series recorded during age rating (Figure 6). Interestingly, we observed a trend for a negative association with subjective value ($p_{corr}=0.062$) between 0.470s and 0.580s after stimulus onset in the OFC and a significant negative association between 0.238s and 0.814s in the (P)HC ($p_{corr}<1.10^{-4}$). The negative association in the OFC was followed by a significant positive correlation with subjective value between 0.829s and 1.094s ($p_{corr}=3.10^{-3}$). We splitted our time window of interest in two halves, given the dynamics observed in the OFC, and confirmed a negative association with value in the 0.5-0.75s time window in both ROIs (OFC: $t(125)=-2.027$, $p=0.045$; (P)HC: $t(145)=-3.89$, $p=2.10^{-3}$; two-sided one-sample t-tests). In the second

time window, we found a significant positive association with value in the OFC only (OFC: t(125)=3.43, p=8.10^{-4}; (P)HC: t(145)=-0.93, p=0.35; two-sided one-sample t-tests).

Thus, the results confirm that the OFC and the (P)HC can reflect value judgments during non-value-related tasks. They also uncover a surprising negative value representation that was most prominent in the (P)HC. Note that the negative correlation is not an artefact due to a difference in the latency of the evoked response, as the tertian split shows an inversion of the response to high- and low-value stimuli (Extended Data 7). To control for a potential contamination of age rating by likeability, we orthogonalized the two regressors and conducted the same regression analysis against power time-series. There was no noticeable difference in the results, with the same difference between the two time windows.

Quadratic coding (evoked activity reflects confidence judgments on ratings)

To test whether the BVS would also reflect second-order judgments (confidence in first-order ratings), we extended the time window of interest to the entire trial, and used time locking to both stimulus onset and motor response (first button pressed to move the cursor along the scale). Power time-series recorded in the two ROIs and two frequency bands were regressed against second-order polynomial extensions of (non-food) likeability rating and (non-food) age rating, collected in the long version of behavioral tasks (Figure 7). We consider quadratic terms as proxies for confidence ratings, since they are both U-shaped functions of first-order rating (see behavioral results). Using this proxy enables comparing regression results with the short versions of behavioral tasks (Extended Data 8a), for which confidence ratings were not acquired.

In the following analyses, we kept the 0.5-1s post-stimulus time window of interest and added an equivalent -0.5-0s time window before first button press (Figure 7 and Extended Data 8). Regression estimates for the quadratic function of likeability rating were significant over the post-stimulus time window in both ROIs (OFC: t(125)=5.55, p=2.10^{-7}; (P)HC: t(145)=4.51, p=1.10^{-5}; two-sided one-sample t-test) and over the pre-response time windows in the OFC (t(125)=4.86, p=3.10^{-6}), but not in the (P)HC (t(145)=0.34, p=0.74).

Together, those results indicate that both OFC and (P)HC high-frequency activity reflected quadratic likeability ratings. The interpretation as a confidence signal (and not a saliency signal) is confirmed by the significant links observed with quadratic age rating. Indeed, the regression against quadratic age rating revealed a significant association in the pre-response time window in both ROIs (OFC: t(125)=2.94, p=4.10^{-3}, (P)HC: t(145)=2.80, p=6.10^{-3}; two-sided one-

sample t-tests). Those results are illustrated in Figure 7b and 7d, for which high-frequency bands (gamma and high-gamma) power time-series were extracted from the post-stimulus and pre-response time windows and binned according to likeability or age rating.

As a control, we replicated the analysis in patients who performed the short version of behavioral tasks (using food items only) and therefore could not have been primed by confidence judgments (Extended Data 8a). The quadratic term was significantly expressed in both time windows (post-stimulus: OFC: $t(323)=4.43$, $p=1.10^{-5}$, (P)HC: $t(255)=4.54$, $p=9.10^{-6}$; pre-response: OFC: $t(323)=5.36$, $p=2.10^{-7}$, (P)HC: $t(255)=6.43$, $p=6.10^{-10}$; two-sided one-sample t-tests). This result suggests that representation of confidence was not induced by the instruction to rate confidence, which was only present in the long version.

As another control, we pooled all judgments together (likeability and age rating) and regressed the signal against the quadratic function of ratings. We compared the results to a regression against actual confidence judgments for patients who performed the long version (Extended Data 8). The results were qualitatively similar, with stronger statistics in the OFC (squared first-order ratings, post-stimulus: $t(125)=5.87$, $p=4.10^{-8}$; pre-response: $t(125)=5.88$, $p=3.10^{-8}$; confidence ratings, post-stimulus: $t(125)=5.05$, $p=1.10^{-6}$; pre-response: $t(125)=3.57$, $p=5.10^{-4}$). This result validates the use of squared rating as a proxy for confidence. Note that significant links with (P)HC activity were also observed in all cases, although not consistently over the entire time windows (see Extended Data 8).

Altogether, the four functional properties were found in the OFC. All but the anticipation property were also observed in the (P)HC (Table 1). For every property, we conducted two-by-two comparisons (between and within the BVS ROIs) of regression estimates averaged over the relevant time windows. Compared to the OFC, the (P)HC only differed regarding the anticipation property ($t(850)=3.37$, $p=1.10^{-3}$, see Table 1). Importantly, there was no significant difference between vmPFC and lOFC, which therefore shared the same four core properties. The same properties were tested in the other regions of the extended BVS: none exhibited the anticipation property but all of them shared the quadratic coding property (Supplementary Table 8).

Discussion

Using a large dataset of iEEG signals recorded in 36 patients with epilepsy during judgment

tasks, we provide information about the BVS regarding 1) its anatomical localization over the whole brain, 2) the dynamical of the different frequency bands, 3) the functional properties of value representation. In the following, we successively discuss these three lines of results.

Delineating the Brain Valuation System

Using direct regression of high-gamma activity against the likeability ratings assigned to food items, we found a large set of brain regions that was significantly reflecting subjective value. Some of these significant ROIs were part of the standard BVS defined from meta-analyses of fMRI studies (e.g., vmPFC), some corresponded to areas where single cells were found to express subjective value (e.g., lOFC) and some were less classically associated with valuation (e.g., hippocampus). The fact that value correlates were similar between vmPFC and lOFC fills a gap between human fMRI and monkey electrophysiology studies. Indeed, previous fMRI studies using similar stimuli did not report value signals in the lOFC. The present results show that the implication of the lOFC in value representation is not dependent on the training procedures or particular tasks used in monkeys, but on the recorded signal (hemodynamic versus electrophysiological activity).

Thus, high-gamma band power, which arguably reflects local neural activation[32,33], seems to provide an interesting bridge between human fMRI activity and monkey spiking activity. Our results are in line with a recent study that reported correlates of reward prospect and receipt in the human OFC high-frequency activity[18], using electrocortigraphy (ECoG). This study raised the question of why most fMRI studies failed to detect any linear link between value correlates and lOFC activity. We can only offer trivial explanations here, such as a higher variability in the location of activated voxels across participants, or a more stringent statistical threshold, related to correction for multiple comparisons over a high number of recorded voxels.

Here, Bonferroni-Holm correction[34] was less stringent, because it was based on the number of ROIs tested (and not the number of voxels). This might partly explain the rather long list of significant associations with subjective value. The issue is even more problematic in typical monkey studies, which investigate only one brain region at a time, and therefore do not correct for multiple comparisons. Indeed, many brain regions have been reported to reflect reward or value across publications[35,36]. In any case, the number of ROIs that were found to correlate with subjective value questions the anatomical specificity of the BVS. This anatomical spread could reflect some functional diversity. Of note, we may have mixed regions involved in the construction of subjective value and those influenced by subjective value. Further investigation

425 is thus needed to tease apart the functional role of the different brain regions associated with
426 subjective value.
427 We also note that some classical BVS regions were not in our list of ROIs significantly
428 reflecting subjective value. One obvious reason is that they were not covered in our sample of
429 recording sites, as was the case for the ventral striatum and posterior cingulate cortex. More
430 generally, the unequal sampling of the AAL atlas ROIs induces differences in the statistical
431 power of the group-level analyses used to test regression. This is why we used the term 'pseudo
432 whole-brain' and why the comparison between regions must be taken with caution.
433

434 **Dynamics of value coding across frequency bands**

435 We observed that subjective value was represented in high-gamma activity of both the OFC and
436 (P)HC, as expected from the pseudo whole-brain analysis. When exploring lower frequencies,
437 the correlation with subjective value was similar between gamma and high-gamma bands for
438 all regions. The correlation was reduced or even negative in low-frequency bands, which we
439 did not analyze further because they were not providing any additional information about
440 subjective values. This finding provides further support to the a priori correspondence between
441 the BOLD signal and high-frequency iEEG activity, since we never observed negative
442 correlation between brain activity and likeability rating in our fMRI studies[9,22] using similar
443 stimuli. We also noted that in this high-frequency band, the main response observed in the
444 vmPFC is a reduced power, with an even stronger reduction for lower values. It is tempting to
445 draw a link with the decrease in BOLD signal that is also observed in the vmPFC following
446 stimulus presentation. Indeed, a typical finding in fMRI studies is that higher stimulus value
447 corresponds to lesser deactivation in the vmPFC (see for example [19]).
448 Focusing on high-frequency bands, we could then examine the separation between the two OFC
449 regions (vmPFC and lOFC) in space and time. Regarding space, we observed a drop in value
450 regression estimates for recording sites situated on the border between the two regions, along
451 the medio-lateral axis. This observation argues against a possible spatial contamination of
452 signals arising from the two regions. Spatial contamination was not very plausible anyway, as
453 the average distance between the two ROI centers was 2-3 cm, whereas LFP signals were shown
454 to aggregate neural activity over less than a 1cm-diameter sphere[37]. Regarding time, we
455 observed that value signals emerged earlier in the lOFC relative to the vmPFC, which could
456 therefore be the final processing stage before selection of the motor response. The analysis of
457 the circulation of information was however limited by the fact that we seldom had all regions

of interest implanted with electrodes in a same patient.

Functional properties of value coding

All core functional properties of value coding that were previously identified with fMRI were replicated here in the vmPFC, and extended to the lOFC high-frequency iEEG activity.

First, we found that subjective values were partially predicted by pre-stimulus OFC activity. A similar result has been recently obtained in both humans and monkeys[19]. The suggestion was that a boost in baseline activity would persist in the evoked activity, resulting in a higher signal and hence a higher value, supposing that value is encoded in the absolute activity level, not in the difference from baseline. Such mechanism would predict that the link with upcoming value persists between baseline and evoked response (i.e., between 0 and 0.5s post-stimulus). We observed that the correlation with value was momentarily lost in this period, but this could be due to high values accelerating the evoked response. This anticipation is an important property that makes value judgment dependent on pre-choice activity, which itself can be influenced by irrelevant contextual features. It may therefore account for psychological phenomena such as misattribution bias or carry-over effects, for instance why we like the food better when the music is pleasant, or why we buy lottery tickets on sunny days.

Second, we found that the value of both food and non-food items was represented not only in OFC, but also in (P)HC activity. This is in line with a wealth of fMRI studies showing that likeability of faces and paintings was correlated with the BVS, and in particular vmPFC activity[22,38], but also other kinds of items such as food[39], trinkets[21] and money[40], consistent with the notion of a 'common neural currency'[23]. This notion is critical for the ability to compare values and choose between items belonging to seemingly incommensurable categories. It is also an important condition for the psychological phenomena mentioned above, which assumes that the values of different features share a same neural representation, which may occasion interferences. We note that regression estimates were lower for the value of non-food items, but this may come from a different range of values in the different categories, or different mapping from value to the rating scale. Although the range of rewards explored is less extensive than in humans, several electrophysiological studies in monkeys reported that OFC neurons are sensitive to the value of non-food items, such as faces of conspecific animals[41,42].

Third, we found that subjective value was expressed in both the OFC and (P)HC activity even during the age rating task. This is replicating the result previously obtained with fMRI[22], and confirms that valuation is a somewhat automatic process. By this we do not mean that the

valuation process is irrepressible, just that valuation does not need an explicit value-based rating or choice task to be triggered. Importantly, the age rating task was performed first, precluding a priming of valuation processes by the likeability rating task. Such automatic valuation might explain a series of 'halo effects' reported in the literature, where the values of irrelevant contextual features contaminate the judgment of target stimuli. We note however that the dynamics of value coding was different from that observed in likeability rating tasks, with an early (surprisingly) negative correlation, followed by the (expectedly) positive correlation, at least in OFC activity. The negative correlation may occur when subjects estimate the age of visual items, and presumably shifts the representation of subjective value to a different neural code. This task-induced recoding may explain why automatic valuation has not been observed in some other fMRI studies using particular decision-making tasks[43,44]. We speculate that electrophysiological recordings would reveal automatic value signals even in these particular paradigms.

Fourth, we found that both OFC and (P)HC activity followed not only linear but also quadratic function of subjective value. The linear link was only observed with likeability, not age rating, confirming the implication of the BVS in valuation, not in assigning a number on a scale. Contrary to the linear link, the quadratic link was observed with both age and likeability ratings, and in both stimulus-locked and response-locked activity. This is consistent with the notion that the quadratic association represents confidence, defined as subjective accuracy of the response, as suggested in our previous fMRI study[26]. Indeed, we verified that confidence ratings were similarly represented in both stimulus-locked and response-locked activity. In other words, the BVS would represent both a first-order value judgment on the stimulus, and a second-order value judgment on the response. This implies that confidence carries an intrinsic value, as we prefer to be accurate than inaccurate. It is in line with a computational model postulating that confidence is precisely the quantity that subjects maximize when giving their response[26]. Confidence itself might be a generic and automatic process, as quadratic association was observed for both age and likeability ratings, even in subjects who were not asked to rate their confidence. This finding is consistent with animal studies claiming that OFC neurons represent confidence, which regulates how much they are willing to wait for the reward that they believe is associated to their response[45]. The co-occurrence of value and confidence representations in the same region may occasion some misattribution, as seen for instance in certain forms of desirability bias (when people feel more confident in their behavior just because the outcome is more rewarding).

Limitations

To our knowledge, this is the first time that the BVS functional properties are investigated through intra-EEG recordings. However, these data have been collected in patients with epilepsy, who were investigated with depth electrodes for a presurgical evaluation. Yet we interpret those data as if they were collected in healthy subjects, making the assumption that epileptic activity did not distort the neural implementation of subjective value. Although we carefully rejected contacts and trials with epileptic activity, this assumption might be questionable. What is reassuring is that most of the results are in accordance with previous investigations in healthy human and non-human primates. Moreover, we investigated patients with different forms of epilepsy, which would induce disparate, or even opposed, distortions of brain activity, unlikely to explain systematic effects. Despite these limitations, we hope that further research will use the opportunity of iEEG recordings to improve our understanding of how subjective value is constructed in the human brain.

Acknowledgements

We thank Jean-Philippe Lachaux, Marwa El Zein, Sebastien Bouret and Emmanuel Procyk for their helpful comments on the analysis of iEEG data, and the ICM for purchasing the acquisition material. This work benefited from the program ’Investissements d’avenir’ (ANR-10-IAIHU-06), from the European Union’s Horizon 2020 Research and Innovation Programme under Grant Agreement No. 720270 (HBP SGA1) and No. 785907 (HBP SGA2), from the LABEX CORTEX (ANR-11-LABX-0042) of Université de Lyon, within the program "Investissements d'Avenir" (ANR-11-IDEX-0007), from IHU CESAME, within the program “Investissements d’Avenir” (ANR-10-IBHU-0003) and from University Grenoble Alpes, within the program “Investissements d’Avenir” (ANR-17-CE37-0018 and ANR-18-CE28-0016). A.L-P. received a PhD fellowship from the Direction Générale de l’Armement and a grant from the LabEx Bio-Psy. The funders had no role in study design, data collection and analysis, decision to publish or preparation of the manuscript.

Author contributions

M.Pes. designed all experiments. A.L-P., J.B. M.Pet. and R.A. collected the data. J.B. provided preprocessing scripts. A.L-P. performed the data analysis. C.A., V.N., S.R. and P.K. did the

intracranial investigation and allowed the collection of iEEG data. K.L. supervised the access to patients in Paris. P.D. provided tools for time-frequency analysis. A.L-P. and M.Pes. wrote the manuscript. All authors discussed the results and commented the manuscript.

Competing interests

The authors declare no competing interests.

References for main text only

1. Krajbich, I., Armel, C. & Rangel, A. Visual fixations and the computation and comparison of value in simple choice. *Nat. Neurosci.* **13**, 1292–1298 (2010).
2. Hunt, L. T. *et al.* Mechanisms underlying cortical activity during value-guided choice. *Nat. Neurosci.* **15**, 470-S3 (2012).
3. O'Doherty, J. P. The problem with value. *Neurosci. Biobehav. Rev.* (2014) doi:10.1016/j.neubiorev.2014.03.027.
4. Juechems, K. & Summerfield, C. Where Does Value Come From? *Trends Cogn. Sci.* **23**, 836–850 (2019).
5. Lopez-Persem, A., Rigoux, L., Bourgeois-Gironde, S., Daunizeau, J. & Pessiglione, M. Choose, rate or squeeze: Comparison of economic value functions elicited by different behavioral tasks. *PLOS Comput. Biol.* **13**, e1005848 (2017).
6. Rangel, A., Camerer, C. & Montague, P. R. A framework for studying the neurobiology of value-based decision making. *Nat. Rev. Neurosci.* **9**, 545–556 (2008).
7. Bartra, O., McGuire, J. T. & Kable, J. W. The valuation system: A coordinate-based meta-analysis of BOLD fMRI experiments examining neural correlates of subjective value. *NeuroImage* **76**, 412–427 (2013).
8. Peters, J. & Büchel, C. Episodic Future Thinking Reduces Reward Delay Discounting through an Enhancement of Prefrontal-Mediotemporal Interactions. *Neuron* **66**, 138–148 (2010).
9. Lebreton, M. *et al.* A Critical Role for the Hippocampus in the Valuation of Imagined Outcomes. *PLoS Biol.* **11**, e1001684 (2013).
10. Schacter, D. L., Addis, D. R. & Buckner, R. L. Remembering the past to imagine the future: the prospective brain. *Nat. Rev. Neurosci.* **8**, 657–661 (2007).
11. Barron, H. C., Dolan, R. J. & Behrens, T. E. J. Online evaluation of novel choices by simultaneous representation of multiple memories. *Nat. Neurosci.* **16**, 1492–1498 (2013).
12. O'Doherty, J., Kringelbach, M. L., Rolls, E. T., Hornak, J. & Andrews, C. Abstract reward and punishment representations in the human orbitofrontal cortex. *Nat. Neurosci.* **4**, 95–102 (2001).
13. Zhang, Z. *et al.* Distributed neural representation of saliency controlled value and category during anticipation of rewards and punishments. *Nat. Commun.* **8**, 1907 (2017).
14. Bouret, S. & Richmond, B. J. Ventromedial and Orbital Prefrontal Neurons Differentially Encode Internally and Externally Driven Motivational Values in Monkeys. *J. Neurosci.* **30**, 8591–8601 (2010).
15. Strait, C. E., Blanchard, T. C. & Hayden, B. Y. Reward Value Comparison via Mutual Inhibition in Ventromedial Prefrontal Cortex. *Neuron* **82**, 1357–1366 (2014).
16. Padoa-Schioppa, C. Orbitofrontal Cortex and the Computation of Economic Value. *Ann. N. Y. Acad. Sci.* **1121**, 232–253 (2007).
17. Tremblay, L. & Schultz, W. Relative reward preference in primate orbitofrontal cortex. *Nature* **398**, 705–708 (1999).
18. Saez, I. *et al.* Encoding of Multiple Reward-Related Computations in Transient and Sustained High-Frequency Activity in Human OFC. *Curr. Biol.* (2018) doi:10.1016/j.cub.2018.07.045.
19. Abitbol, R. *et al.* Neural Mechanisms Underlying Contextual Dependency of Subjective Values: Converging Evidence from Monkeys and Humans. *J. Neurosci.* **35**, 2308–2320 (2015).
20. Vinckier, F., Rigoux, L., Oudiette, D. & Pessiglione, M. Neuro-computational account of how mood fluctuations arise and affect decision making. *Nat. Commun.* **9**, 1708 (2018).
21. Chib, V. S., Rangel, A., Shimojo, S. & O'Doherty, J. P. Evidence for a Common Representation of Decision Values for Dissimilar Goods in Human Ventromedial Prefrontal Cortex. *J. Neurosci.* **29**, 12315–12320 (2009).
22. Lebreton, M., Jorge, S., Michel, V., Thirion, B. & Pessiglione, M. An Automatic Valuation System in the

Human Brain: Evidence from Functional Neuroimaging. *Neuron* **64**, 431–439 (2009).
23. Levy, D. J. & Glimcher, P. W. The root of all value: a neural common currency for choice. *Curr. Opin. Neurobiol.* (2012) doi:10.1016/j.conb.2012.06.001.
24. Levy, I., Lazzaro, S. C., Rutledge, R. B. & Glimcher, P. W. Choice from Non-Choice: Predicting Consumer Preferences from Blood Oxygenation Level-Dependent Signals Obtained during Passive Viewing. *J. Neurosci.* **31**, 118–125 (2011).
25. De Martino, B., Fleming, S. M., Garrett, N. & Dolan, R. J. Confidence in value-based choice. *Nat. Neurosci.* **16**, 105–110 (2013).
26. Lebreton, M., Abitbol, R., Daunizeau, J. & Pessiglione, M. Automatic integration of confidence in the brain valuation signal. *Nat. Neurosci.* **18**, 1159–1167 (2015).
27. Tzourio-Mazoyer, N. *et al.* Automated Anatomical Labeling of Activations in SPM Using a Macroscopic Anatomical Parcellation of the MNI MRI Single-Subject Brain. *NeuroImage* **15**, 273–289 (2002).
28. Logothetis, N. K., Pauls, J., Augath, M., Trinath, T. & Oeltermann, A. Neurophysiological investigation of the basis of the fMRI signal. *Nature* **412**, 150–157 (2001).
29. Scheeringa, R. *et al.* Neuronal Dynamics Underlying High- and Low-Frequency EEG Oscillations Contribute Independently to the Human BOLD Signal. *Neuron* **69**, 572–583 (2011).
30. Ray, S., Crone, N. E., Niebur, E., Franaszczuk, P. J. & Hsiao, S. S. Neural Correlates of High-Gamma Oscillations (60-200 Hz) in Macaque Local Field Potentials and Their Potential Implications in Electrocorticography. *J. Neurosci.* **28**, 11526–11536 (2008).
31. Bastin, J. *et al.* Direct recordings in human cortex reveal the dynamics of gamma-band [50–150Hz] activity during pursuit eye movement control. *NeuroImage* **63**, 339–347 (2012).
32. Jerbi, K. *et al.* Task-related gamma-band dynamics from an intracerebral perspective: Review and implications for surface EEG and MEG. *Hum. Brain Mapp.* **30**, 1758–1771 (2009).
33. Lachaux, J.-P., Axmacher, N., Mormann, F., Halgren, E. & Crone, N. E. High-frequency neural activity and human cognition: Past, present and possible future of intracranial EEG research. *Prog. Neurobiol.* **98**, 279–301 (2012).
34. Holm, S. A Simple Sequentially Rejective Multiple Test Procedure. *Scand. J. Stat.* **6**, 65–70 (1979).
35. Wallis, J. D. & Kennerley, S. W. Heterogeneous reward signals in prefrontal cortex. *Curr. Opin. Neurobiol.* **20**, 191–198 (2010).
36. Hunt, L. T. & Hayden, B. Y. A distributed, hierarchical and recurrent framework for reward-based choice. *Nat. Rev. Neurosci.* **18**, 172–182 (2017).
37. Buzsáki, G., Anastassiou, C. A. & Koch, C. The origin of extracellular fields and currents — EEG, ECoG, LFP and spikes. *Nat. Rev. Neurosci.* **13**, 407–420 (2012).
38. Harvey, A. H., Kirk, U., Denfield, G. H. & Montague, P. R. Monetary Favors and Their Influence on Neural Responses and Revealed Preference. *J. Neurosci.* **30**, 9597–9602 (2010).
39. Hare, T. A., Camerer, C. F. & Rangel, A. Self-Control in Decision-Making Involves Modulation of the vmPFC Valuation System. *Science* **324**, 646–648 (2009).
40. Kable, J. W. & Glimcher, P. W. The neural correlates of subjective value during intertemporal choice. *Nat. Neurosci.* **10**, 1625–1633 (2007).
41. Watson, K. K. & Platt, M. L. Social Signals in Primate Orbitofrontal Cortex. *Curr. Biol.* **22**, 2268–2273 (2012).
42. Azzi, J. C. B., Sirigu, A. & Duhamel, J.-R. Modulation of value representation by social context in the primate orbitofrontal cortex. *Proc. Natl. Acad. Sci.* **109**, 2126–2131 (2012).
43. Grueschow, M., Polania, R., Hare, T. A. & Ruff, C. C. Automatic versus Choice-Dependent Value Representations in the Human Brain. *Neuron* (2015) doi:10.1016/j.neuron.2014.12.054.
44. Grabenhorst, F. & Rolls, E. T. Selective attention to affective value alters how the brain processes taste stimuli. *Eur. J. Neurosci.* **27**, 723–729 (2008).
45. Mainen, Z. F. & Kepecs, A. Neural representation of behavioral outcomes in the orbitofrontal cortex. *Curr. Opin. Neurobiol.* **19**, 84–91 (2009).

Figure legends

Figure 1 – Behavioral tasks and results

Top. Behavioral tasks. Successive screens show example trials. In the age rating task **(a)** of non-food items (faces or paintings, framed in dark grey), patients provided judgments using

analog scales between 0 and 80 years for the age of faces and between 1400 and 2000 years for the date of paintings. Confidence in the first-order rating was reported on a continuous scale going from 'not at all confident' to 'totally confident'. In the likeability rating task **(b)**, patients indicated on an analog scale how much they liked the item from -10 to 10. The item could be food (red frame) or non-food (face or painting, dark grey). In the choice task **(c)**, two items presented in the rating tasks were displayed side by side on the screen and patients had to select the one they preferred. **Bottom**. Behavioral results. In the rating tasks, the quadratic link was positive between confidence and age or likeability rating (**d-e**, top), and negative between RT and age or likeability rating (**d-e**, bottom), for both food (red dots) and non-food (black dots) items. In the choice tasks, the difference between likeability ratings (option values V) predicted both choice rate (**f**, top) and choice RT (**f**, bottom), for both food (red dots) and non-food (black dots) items. n=X indicates the number of patients tested for each result. Diamonds show binned data averaged across patients. Error bars are inter-subject S.E.M. Lines corresponds to polynomial fit for d and e, logistic fit for top f and linear fit for bottom f.

Figure 2 – Anatomical locations of recording sites in the whole dataset

Top. Sagittal slices of a brain template on which were superimposed the approximate locations of recording sites in 36 epileptic patients. Each dot (2 by 2 voxels) represents one recording site (i.e., a bipole). **Bottom**. Axial slices of a brain template that represents all AAL areas including at least 9 recording sites. Color coding (from dark red to light yellow) indicates the number of recording sites in each dot (top) or each area (bottom). x and z coordinates refer to the MNI atlas.

Figure 3 – Time-frequency investigation of the BVS evoked response

a. Anatomical localization of the vmPFC (red, first row), lOFC (blue, second row), hippocampus (green, third row) and PHC (brown, fourth row). All N recording sites located in those areas were included in the ROI analysis. **b**. Time-frequency analysis of the evoked response following visual item onset (dashed vertical line) averaged over all N recording sites and all food likeability rating trials. Hotter colors indicate higher power. Horizontal dashed lines indicate boundaries between frequency bands that are investigated in panels c and d. Horizontal thick black line between 0.5 and 1 s indicates the time window investigated in panels c. **c.** Regression estimates of power against food likeability rating, averaged over the 0.5-1 s window, for each frequency band defined in b. Center lines, center circles, box limits, whiskers and points of the box plots respectively represent median, mean, interquartile range, extreme data points and outliers of the data distribution from the N recording sites. Black stars indicate significance ($p<0.05$) of regression estimates (one-sample two-sided t-test) '+' indicates a trend with $p=0.06$). **d**. Time course of regression estimates for the gamma and high-gamma frequency band. Solid (dashed) lines indicates mean (SEM) across power time series. Stars indicate significant time points (one-sample two-sided t-test after cluster-wise correction, $p<0.05$). Shaded areas highlight the time window of interest used in c and in following analyses. n=number of power time series.

Figure 4 – Anticipation of value signaling during pre-stimulus period in the BVS.

Left. Time course of the regression estimates of OFC (top, pooling vmPFC and lOFC) and (P)HC (bottom, pooling hippocampus and PHC) activity against food likeability rating. Solid

lines represent means across recording sites and high-frequency bands (gamma and high-gamma). Dashed lines represent SEM across power time series. Double arrows indicate the tested pre-stimulus time window. Stars indicate significance of regression estimates against 0 (after cluster-wise correction); ns indicates non-stignifiance. n is the number of power time series included in the analysis. Shaded areas indicate time windows used for statistical report in the text. Right. Regions of interest included in each time course. Red: vmPFC, blue: lOFC, green: hippocampus, brown: PHC.

Figure 5 – Generality of value signaling in the BVS.

a. Time course of regression estimates for OFC (top, purple) and (P)HC (bottom, yellow) high-frequency bands (gamma and high-gamma) activity against food item likeability rating, in the subset of patients who were administered the long version of behavioral tasks. **b**. Time course of regression estimates in the same ROIs and frequency bands, against non-food item (painting and face) likeability rating, recorded during the likeability rating task. This analysis is meant to assess the generality of value signaling (extending from food to non-food categories). Illustrative screens of the behavioral tasks (food item likeability rating, non-food item likeability rating) are depicted on the left side. Location of ROIs is illustrated on the right side. Shaded areas correspond to the time window of interest (divided in two halves). Dashed lines represent SEM across recording sites. Stars represent significance of regression estimates tested against 0 (two-sided one-sample t-test, $p<0.05$, after cluster-wise correction). n is the number of power time series included in the analysis.

Figure 6 – Automaticity of value signaling in the BVS

Plots show time-resolved regression of OFC (top, purple) and (P)HC (bottom, yellow) high-frequency band (gamma and high-gamma) power time series against non-food item (painting and face) likeability rating, recorded during the age rating task. This analysis is meant to assess the automaticity of value signaling (expressed during judgement of orthogonal dimensions such as age). Illustrative screens of the behavioral tasks (food item likeability rating, non-food item likeability rating) are depicted on the left side. Location of ROIs is illustrated on the right side. Shaded areas correspond to the time window of interest (divided in two halves). Dashed lines represent SEM across recording sites. Stars represent significance of regression estimates tested against 0 after cluster-wise correction (two-sided one-sample t-test, $p<0.05$, cluster correction, '+' indicates a trend with $p=0.06$). n is the number of power time series included in the analysis.

Figure 7 – Quadraticity of value signaling in the BVS.

High-frequency band (gamma and high-gamma) power time series extracted from the OFC ROI (pooling vmPFC and lOFC data) were regressed against non-food squared likeability (top) and squared age (bottom). **a**. Plots show the time course of regression estimates locked on stimulus onset (left) and first button press (right). Stars represent significance of regression estimates tested against 0 after cluster-wise correction (two-sided one-sample t-test, $p<0.05$). Shaded areas depict time windows for which statistical results are reported in the text. Solid (dashed) lines indicates mean (SEM) across recording sites. **b**. Plots show high-frequency power in the OFC as a function of likeability or age rating. Circles (error bars) represent the mean (SEM) of bins, solid (and dashed) lines represent the mean (and SEM) of second-order polynomial fit. Significant linear and quadratic regressors are indicated as red p-values above

the graphs (two-sided one-sample t-test). n indicates the number of time series used in each analysis. **c** and **d** are the same analyses as in a and b, applied to the (P)HC ROI (pooling hippocampal and para-hippocampal data).

Table 1: Summary of the BVS functional properties

		ANTICIPATION	GENERICITY	AUTOMATICITY		QUADRATICITY
				0.5 – 0.75s	0.75 -1s	
OFC	n	450	126	126	126	450
	mean	0.011	0.015	-0.012	0.022	0.018
	SEM	0.005	0.005	0.006	0.007	0.003
	df	449	125	125	125	449
	t	2.380	2.620	-2.027	3.430	6.69
	p	0.018	0.010	0.045	8.10^{-3}	7.10^{-11}
(P)HC	n	402	146	146	146	402
	mean	-0.007	0.012	-0.0241	-0.008	0.017
	SEM	0.004	0.005	0.006	0.009	0.003
	df	401	145	145	145	401
	t	-1.570	2.340	-3.892	-0.930	6.29
	p	0.120	0.020	2.10^{-4}	0.350	6.10^{-10}
OFC vs (P)HC	mean	0.021	0.017	0.012	0.012	0.006
	SEM	0.006	0.009	0.009	0.016	0.004
	df	850	270	270	270	850
	t	3.365	1.958	1.380	0.758	1.693
	p	0.001	0.051	0.169	0.449	0.091
vmPFC vs lOFC	mean	0.004	-0.013	0.004	0.020	0.010
	SEM	0.009	0.012	0.013	0.015	0.006
	df	448	124	124	124	448
	t	0.415	-1.050	0.313	1.303	1.793
	p	0.678	0.296	0.755	0.195	0.074

The table provides summary statistics for each functional property tested separately (two-sided one-sample Student's test) in OFC and (P)HC activity (top) and for two-by-two comparisons (linear mixed-effects models) between and within ROIs (bottom). Abbreviations: SEM: standard error of the mean; df, t, p: degree of freedom, t-value and p-value of the test. In bold are the significant results. Anticipation: test of food likeability regression estimates in the -0.2-0s pre-stimulus activity. Genericity: test of non-food likeability regression estimates in the 0.5-1.0s post-stimulus activity. Automaticity: test of the non-food likeability regression estimates during the age rating task in the 0.5-0.75s and 0.75-1s time windows after the stimulus onset. Quadraticity: test of squared food likeability regression estimates during the food likeability rating task in the -0.5-0s time window before the response onset. n indicates the number of power time series included in the analysis.

Methods

Patients and recordings

All 36 patients (37.9 ± 10.7 years old, 21 females, see demographical details in Supplementary Table 1) were suffering from drug-resistant focal epilepsy and gave written, informed consent prior to their inclusion in the study. They were tested in three different epilepsy departments: Lyon (n=18), Grenoble (n=7) and Paris (n=11). In Lyon and Grenoble, the implantation of electrodes and the participation of patients to cognitive tasks received approval from the Institutional Review Board and by the National French Science Ethical Committee (CPP 09-CHUG-12, study 0907) and from the French National Agency for Medicines and Health Products Safety (ANSM no: 2009-A00239-48). Patients underwent intracerebral recordings by means of stereotactically implanted[46] multilead depth electrodes (sEEG). For each patient, 12 to 18 semi-rigid electrodes were implanted depending on the patient; each electrode had a diameter of 0.8 mm and comprised 6 to 18 leads of 2 mm, 1.5 mm apart (Dixi, Besançon, France), depending on the target region. The electrode contacts were identified on each individual stereotactic scheme, and then anatomically localized using the proportional atlas of Talairach & Tournoux[47], after linear-scale adjustment to correct for size differences between the patient's brain and the brain template in the Talairach atlas. Neuronal recordings were conducted using an audio–video-EEG monitoring system (Micromed, Treviso, Italy), which allowed simultaneous recording of 128 or 256 depth-EEG channels sampled at 512 Hz [0.1–200 Hz bandwidth]. One of the contact sites located in the white matter was used as a reference. In Paris, the implantation of electrodes and the participation of patients to cognitive tasks received approval from local ethic committee (CPP Paris VI, Pitié-Salpêtrière Hospital, INSERM C11-16). The electrodes (AdTech®, Wisconsin) were 4-12 platinum contact electrodes, 1mm diameter and 1.6mm length, with nickel-chromium wiring. Neural recordings were conducted with Neuralynx (ATLAS, Neuralynx®, Inc., Bozeman, MO). Spatial localizations were determined on the basis of postimplant computed tomography scans coregistered with preimplant 1.5T MRI scans. Placement of the electrodes was determined by clinical criteria. The reference electrode was defined as the one with least activity, if possible in the white matter. Signal was band-pass filtered between 0.1 Hz and 1000 Hz. Localization of electrodes has been recovered automatically using the Epiloc toolbox (Version V1) developed by the STIM (http://pf-stim.cricm.upmc.fr/) engineering facility in the ICM (Institut du Cerveau et de la Moelle épinière, (http://icm-institute.org/fr/cenir-stim-stereotaxy-core-facility-techniques-images-models/)[48].

Before analysis, all signals were re-referenced to their nearest neighbor on the same electrode, yielding a bipolar montage.

Blinding and randomization

There is no comparison between groups or conditions in our design and therefore no need for randomization or blind testing. The tasks were performed in the same order by every patient, but sequence of item presentation was randomized.

Experimental tasks

Long version

In Paris, patients performed the long version of behavioral tasks, which were programmed on a PC using Matlab 2013 and the Cogent 2000 (Wellcome Department of Imaging Neuroscience, London, UK) library of Matlab functions for stimulus presentation.

The long version of the task comprised three phases and all trials started with a fixation cross lasting for 1500 ± 500 ms.

First was the "Age Rating & Confidence task", composed of 120 trials divided in two blocks of 60 trials (one with faces and the other with paintings), whose order was counterbalanced across patients. On every trial, an image appeared on screen and patients had to rate how old the presented stimulus was, on a 21-step scale that was adapted to the stimulus category (face or painting). After validation of the age judgment, another 100-step (almost continuous) rating scale was displayed, on which participants were asked to indicate how confident they were, between "Not at all" and "Totally", about their first-order rating, which was reminded on the screen ("You gave a rating of *X*"). In all rating tasks, the answer was given with the right hand. The cursor initial position was randomized and it could be moved by pressing left and right arrows on the keyboard and then validated by pressing the space bar. Once validated, the next trial started. The order of stimulus presentation was randomized, separately for each participant.

Second, in the "Likeability Rating & Confidence task", patients were shown in three different blocks the same faces and paintings, with the addition of a block presenting food items (60 trials in each block). They were asked to indicate on a 21-step scale graduated from -10 to 10 how much they liked the stimulus presented on screen. Each likeability rating was followed by a confidence rating, presented in the same way as during the age rating task.

Third, patients completed three blocks of 60 trials each of a forced binary choice task among the stimuli that were previously rated. After the fixation cross, two pictures belonging to the same category (food, face or painting) were displayed on each side of the screen. Patients had to choose the one they preferred by pressing the left or right arrow of the keyboard. The selected option was framed to give patients a visual feedback on their choice. Note that one patient did not complete the tasks on face stimuli (age, likeability and choice) but we nonetheless included his data in the analysis.

Short version

In Lyon and Grenoble, patients performed the short version of behavioral tasks, composed of one likeability rating task without confidence judgment and one binary choice task, both restricted to food items. All food stimuli were displayed using Presentation software (version 16.5, Neurobehavioral Systems, Albany, CA) on a 17 CRT monitor at 85 Hz. The EEG-acquisition PC was synchronized to the stimulation PC via a TTL pulse signaling stimulus onset. All aspects of the food rating and choice tasks were the same as previously described, except that they completed 120 trials for each task instead of 60. The order of stimulus presentation was also randomized, separately for each participant. Note that one patient did not complete the choice task but we nonetheless included his rating task data in the analysis.

3 patients in Grenoble completed the long version of the task, using the setup of the short version (Presentation software and 85 Hz monitor), but the experimental details of the long version. Among them, one completed both versions (short then long on another day).

Behavioral analysis

Unless otherwise specified, all dependent variables (raw, *z*-scored or binned behavioral measures and regression estimates) were analyzed at the subject level and tested for significance at the group level (random-effect analysis) using two-tailed paired *t*-tests. All regressions were performed on *z*-scored independent and dependent variables. All variables were tested for normality using the Kolmogorov–Smirnov (K-S) test (all $p>0.05$). All statistical analyses were performed with Matlab Statistical Toolbox (Matlab R2016a, The MathWorks, Inc., USA).

Electrophysiological analysis

Collected iEEG signals were analyzed with the software package for electrophysiological analysis (ELAN-Pack, Elan for Ubuntu-10-x86_64) developed in Lyon (INSERM U1028, Lyon, France), with the addition of Fieldtrip[49] (version r7276, http://www.ru.nl/neuroimaging/fieldtrip) and homemade Matlab algorithms. Bipolar

derivations were computed between adjacent contacts to suppress contributions from non-local assemblies and ensure that iEEG signals could be considered as originating from a cortical volume centered within the two contacts[32]. 50 Hz noise was removed from the data using a notch filter. Data were then inspected in order to remove electrodes with suspected epileptic focus from the analysis: windows of 50 ms around time points with intensity higher or lower than five times the standard deviation of the average signal were replaced by NaN values, in order to exclude those points from the following analyses. Data normality was assessed with the Kolmogorov–Smirnov (K-S) test prior to any statistical test (all $p>0.05$).

AAL restructuration

The AAL (Automated Anatomical Labeling) Atlas was used to label each contact located in the MNI space. However, in order to get comparable size and hence statistical power, brain regions larger than 2000 voxels where separated in two brain regions along the larger axis (until all regions had a volume inferior to 2000 voxels). On the contrary, brain regions smaller than 1000 voxels were combined (as for example the gyrus rectus or the frontal medial orbital brain area). We nevertheless kept some regions with less than 1000 voxels, because it would make no sense to combine them with their neighbors. These regions were the bilateral amygdala (220 voxels), the bilateral Heschl gyrus (225 voxels) and the bilateral pallidum (473 voxels). The new atlas included 115 areas (see Supplementary Table 2), with an average volume of 1771 +/- 124 voxels. Only the 77 regions with at least 9 recording sites were retained for statistical analyses. Our dataset included a total of 4273 recording contacts in 36 patients. Contacts with low-quality signals were removed and bipolar montages were computed for each pair of adjacent contacts. Among the 3440 remaining recording sites, 3194 were located within one of these 77 regions and were therefore kept for analysis. Coordinates of recording sites were computed as the mean of the MNI coordinates of the two contacts composing the bipole.

The term ‘pseudo’ acknowledges the fact that comparison between regions is heavily biased by differences in the number of recording sites, which conditions the statistical power of the test performed to detect value signals.

Regions of interest definition

The vmPFC ROI (73 sites, in red on Figure 3a and Supplementary Table 2) was defined as the gyrus rectus plus the fronto-medial part of orbitofrontal cortex bilaterally. The lOFC ROI (152 sites, in blue on Figure 3a and Supplementary Table 2) was defined as the bilateral central and

lateral parts of the orbitofrontal cortex (AAL labels: frontal superior orbital and frontal middle orbital, respectively). The hippocampus (140 sites) and PHC (61 sites) ROIs correspond to those defined in the AAL (in green and brown on Figure 3a, Supplementary Figure 3 and Supplementary Table 2).

Extraction of frequency envelopes

To determine the time course of a priori high-gamma band power, continuous iEEG signals were first band-pass filtered in multiple successive 10Hz-wide frequency bands (e.g., 11 bands from [50–60 Hz] to [140–150 Hz]) using a zero-phase shift non-causal finite impulse filter with 0.5 Hz roll-off. Next, for each band-pass filtered signal we computed the envelope using standard Hilbert transform. The obtained envelope had a sampling rate of 64 Hz (i.e., one time sample every 15.625 ms). Again, for each frequency band, this envelope signal (i.e., time varying amplitude) was divided by its mean across the entire recording session and multiplied by 100. This yields instantaneous envelope values expressed in percentage (%) of the mean. Finally, the envelope signals computed for each consecutive frequency band were averaged together to provide a single time series (the high-gamma band envelope) across the entire session. By construction, the mean value of that time series across the recording session is equal to 100. Note that computing the Hilbert envelopes in 10Hz sub-bands and normalizing them individually before averaging over the broadband interval allows us to counteract a bias toward the lower frequencies of the interval induced by the 1/f drop-off in amplitude. Finally, the obtained time series were smoothed using a sliding window of 250 ms to get rid of potential artifacts.

The envelopes of theta, alpha, beta and gamma bands were extracted in a similar manner as the high-gamma frequency except that steps were 1 Hz for theta and alpha and 5 Hz for beta and gamma. The ranges corresponding to the different frequency bands were determined according to the average time-frequency profiles observed across patients and contacts in the selected region of interest (see Figure 3). High-gamma band was defined as 70-150 Hz, gamma as 35-70 Hz, beta as 15-35 Hz, alpha as 8-15 Hz and theta as 4-8 Hz.

General Linear Models

Frequency envelopes of each bipolar contact were epoched on each trial with two time locking (stimulus onset: -500 to 1500 ms, and first keypress: -1500 to 1500 ms). Each time series was regressed against the variables of interest to obtain a regression estimate per time point and

contact.

In all GLMs, power Y (normalized envelope) was regressed across trials against rating R (normalized within patients and tasks R) at every time point:

$Y = \alpha + \beta R$

With β corresponding to the regression estimate on which statistical tests are conducted. R corresponds to:

- Food likeability rating during the likeability rating task in the figures 3, 4, and 5a, and Extended Data 4, 5, 6.
- Painting and face likeability rating during the likeability rating task in figure 5b
- Painting and face likeability rating during the age rating task in figure 6.
- Squared likeability, age and confidence ratings during likeability, age and confidence rating tasks in Figure 7 and Extended Data 8c (Judgment^2)
- Confidence rating (on age and likeability rating) in Extended Data 8c (Confidence rating).

For the investigation of quadratic coding, each power time-series Y was regressed against second-order polynomial extensions of rating:

$Y = \alpha + \beta_1 R + \beta_2 R^2$

With β_1 and β_2 corresponding to the « linear term » and « quadratic term » regression estimates.

To assess the contribution of the different frequency bands to value representation, we used the following GLM:

$R = \beta_{H\gamma} * Y(H\gamma) + \beta_{\gamma} * Y(\gamma) + \beta_{\beta} * Y(\beta) + \beta_{\alpha} * Y(\alpha) + \beta_{\theta} * Y(\theta)$

With β corresponding to the regression estimates each power time series Y in the high-gamma, gamma, beta, alpha and theta frequency bands. This GLM was compared to the 7 following GLMs:

$R = \beta_{H\gamma} * Y(H\gamma) + \beta_{\gamma} * Y(\gamma)$

$R = \beta_{H\gamma} * Y(H\gamma) + \beta_{\gamma} * Y(\gamma) + \beta_{\beta} * Y(\beta)$

$R = \beta_{H\gamma} * Y(H\gamma) + \beta_{\gamma} * Y(\gamma) + \beta_{\alpha} * Y(\alpha)$

$R = \beta_{H\gamma} * Y(H\gamma) + \beta_{\gamma} * Y(\gamma) + \beta_{\theta} * Y(\theta)$

$R = \beta_{H\gamma} * Y(H\gamma) + \beta_{\gamma} * Y(\gamma) + \beta_{\beta} * Y(\beta) + \beta_{\alpha} * Y(\alpha)$

$R = \beta_{H\gamma} * Y(H\gamma) + \beta_{\gamma} * Y(\gamma) + \beta_{\beta} * Y(\beta) + \beta_{\theta} * Y(\theta)$

$R = \beta_{H\gamma} * Y(H\gamma) + \beta_{\gamma} * Y(\gamma) + \beta_{\alpha} * Y(\alpha) + \beta_{\theta} * Y(\theta)$

The model comparison was conducted using the VBA toolbox (version V3, Variational Bayesian Analysis toolbox, available at http://mbb-team.github.io/). Log-model evidence obtained in each recording site was taken to group-level random-effect Bayesian model

971 selection (RFX-BMS) procedure[50,51]. RFX-BMS provides an exceedance probability (Xp) that
972 measures how likely it is that a given model is more frequently implemented, relative to all the
973 others considered in the model space, in the population from which samples were drawn.
974
975 *Statistical assessment*
976 No statistical methods were used to pre-determine sample size but our sample size is much
977 larger than those reported in typical publications using iEEG[18,52].
978 For all GLMs, significance of regressors was assessed using one-sample two-tailed t-tests. T-
979 values and p-values of those tests are reported in the results sections. Effect sizes correspond to
980 standardized linear regression coefficients obtained with the matlab function glmfit. When
981 comparing two regions, significance was assessed using linear mixed-effects models, that
982 included patient ID as a random factor. When comparing frequencies, significance was assessed
983 using a two-tailed paired t-test.
984 When no a priori time window was selected, significance was assessed through permutation
985 tests. The pairing between power and regressor values across trials was shuffled randomly 2000
986 times. The maximal cluster-level statistics (the sum of t-values across contiguous time points
987 passing a significance threshold of 0.05) were extracted for each shuffle to compute a 'null'
988 distribution of effect size across a time window of -0.2 to 1.5 s around stimulus presentation, or
989 -1 to 1 s around first keypress. For each significant cluster in the original (non-shuffled) data,
990 we computed the proportion of clusters with higher statistics in the null distribution, which is
991 reported as the 'cluster-level corrected' p-value (p_{corr})[53].
992
993 *Whole-brain analysis*
994 For each region included in the pseudo whole-brain analysis, a t-value was computed across all
995 recording sites for each time point after stimulus onset, independently of patient identity (fixed-
996 effect second-level analysis). This allowed the inclusion of brain regions with a small number
997 of recording sites. Significance of each brain region was assessed by permutation tests on
998 clusters longer than 80 ms with a corrected p=0.05, as describe above. Significance threshold
999 was then corrected for multiple comparisons across brain regions, using Bonferroni-Holm
1000 correction. The minimal duration of a cluster was set in order to avoid any transitory false
1001 positive effect.
1002

Time-frequency analysis

Time-frequency analyses were carried out using the FieldTrip toolbox for MATLAB. Spectral powers were estimated using a ‘‘multitapering’’ time-frequency transform (Slepian tapers, lower frequency range: 4–32 Hz, 6 cycles and 3 tapers per window, higher frequency range: 32-200 Hz, fixed time windows of 240 ms, 4 to 31 tapers per window). This approach uses a constant number of cycles across frequencies up to 32 Hz (hence a time window whose duration decreases when frequency increases), and a fixed time window with an increasing number of tapers above 32 Hz to obtain more precise power estimates by adaptively increasing smoothing at high frequencies.

Cross-correlation analysis

To assess the temporal dynamics of value representation across regions (Supplementary Figures 1 and 2), we searched for correlations between every possible combination of regression estimates obtained for (non-smoothed) high-gamma band power against food likeability. All possible pairs of electrodes implanted in a same patient were tested. For each pair, we computed one Pearson’s correlation coefficient per time lag, from 0 to 0.5 s with steps of 16 ms (time resolution of the preprocessed data). Correlation coefficients for a given pair of regions were then tested for significance, pooling pairs recorded in different patients (fixed effect). The null distribution of effect size was established using 1000 permutation of pair labels.

Decoding analysis

All high-frequency signals recorded in a given ROI during the food likeability rating task were combined in large time by trial matrices. Trials were sorted into high and low ratings using a tertian split. At evey time point, a logistic classifier was trained on 90% of trials, and tested on the remaining 10%, with 100 different partitions. The average accuracy per time point is displayed in Extended Data 6. The same procedure was applied on 1000 label permutations to get a random decoding score per time point. Cluster-correction was then applied on the time-window showing significance.

The tertian split was also used to assess the dynamics of high-gamma band evoked response and displayed in Extended Data 7, first row. A similar procedure was applied to high-gamma

signals recorded during the non-food age rating task and provided the results displayed in Extended Data 7, second row.

Data availability

The data that support the findings of this study are available from the corresponding author (A.L-P.) upon request.

Code availability

The custom code used to generate the figures and statistics are available from the corresponding author (A.L-P.) upon request.

Reporting Summary

Further information on research design is available in the Life Sciences Reporting Summary linked to this article.

Methods-only references

46. Lachaux, J. P., Rudrauf, D. & Kahane, P. Intracranial EEG and human brain mapping. *J. Physiol.-Paris* **97**, 613–628 (2003).
47. Talairach, J. & Tournoux, P. Co-planar stereotaxic atlas of the human brain. 3-Dimensional proportional system: an approach to cerebral imaging. (1988).
48. Perez-Garcia, F. *et al.* Automatic segmentation of depth electrodes implanted in epileptic patients: a modular tool adaptable to multicentric protocols. *Epilepsia* **56**, 227 (2015).
49. Oostenveld, R., Fries, P., Maris, E. & Schoffelen, J.-M. FieldTrip: Open Source Software for Advanced Analysis of MEG, EEG, and Invasive Electrophysiological Data. *Computational Intelligence and Neuroscience* https://www.hindawi.com/journals/cin/2011/156869/ (2011) doi:10.1155/2011/156869.
50. Rigoux, L., Stephan, K. E., Friston, K. J. & Daunizeau, J. Bayesian model selection for group studies — Revisited. *NeuroImage* **84**, 971–985 (2014).
51. Stephan, K. E., Penny, W. D., Daunizeau, J., Moran, R. J. & Friston, K. J. Bayesian model selection for group studies. *NeuroImage* **46**, 1004–1017 (2009).
52. Bastin, J. *et al.* Direct Recordings from Human Anterior Insula Reveal its Leading Role within the Error-Monitoring Network. *Cereb. Cortex* bhv352 (2016) doi:10.1093/cercor/bhv352.
53. Maris, E. & Oostenveld, R. Nonparametric statistical testing of EEG- and MEG-data. *J. Neurosci. Methods* **164**, 177–190 (2007).

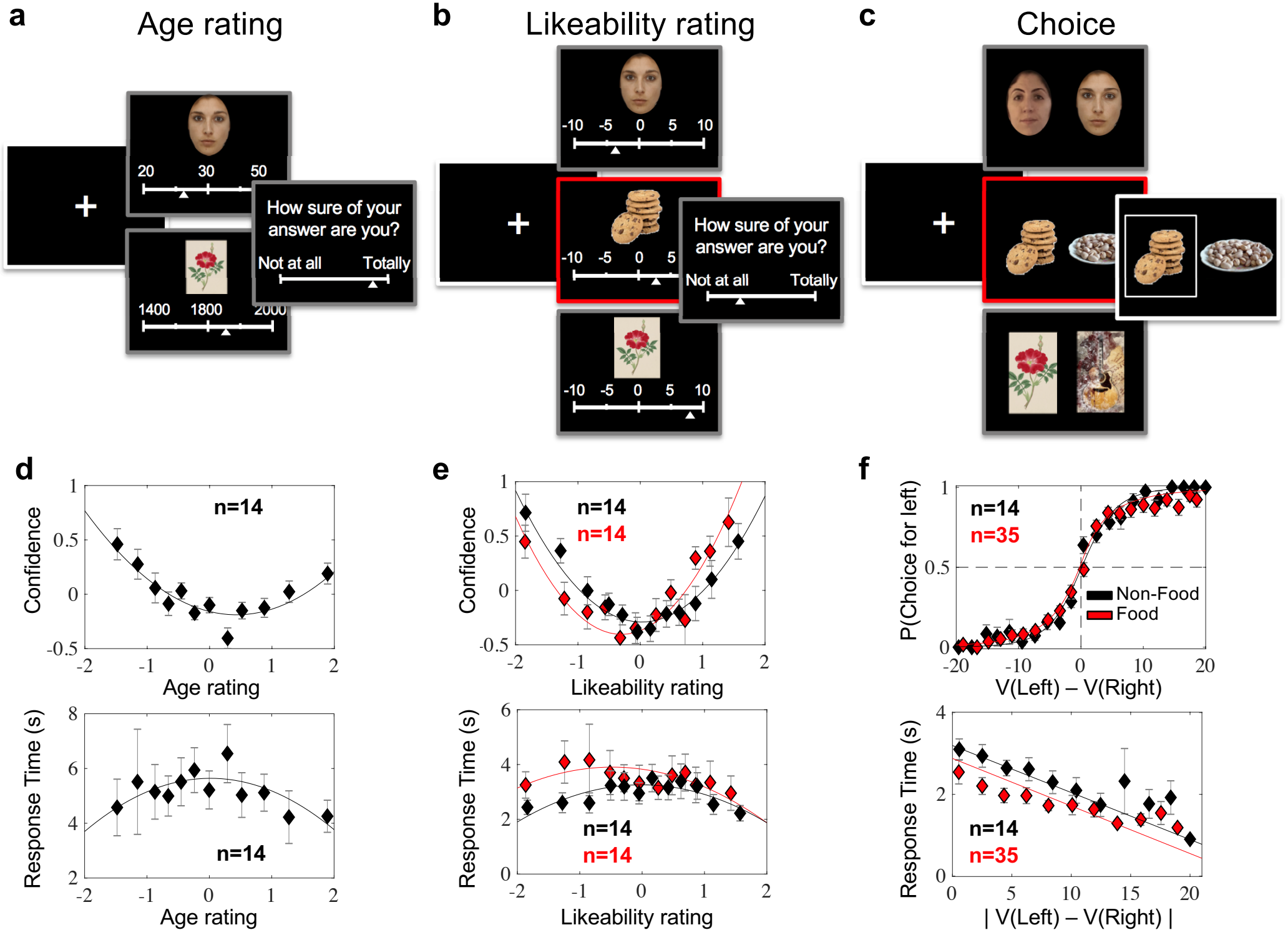
a
Age rating
20 30 50
How sure of your answer are you?
Not at all Totally
1400 1800 2000
b
Likeability rating
-10 -5 0 5 10
How sure of your answer are you?
Not at all Totally
c
Choice
d
Confidence
n=14
Age rating
Response Time (s)
n=14
Age rating
e
Confidence
n=14
n=14
Likeability rating
Response Time (s)
n=14
n=14
Likeability rating
f
P(Choice for left)
n=14
n=35
Non-Food
Food
V(Left) – V(Right)
Response Time (s)
n=14
n=35
| V(Left) – V(Right) |

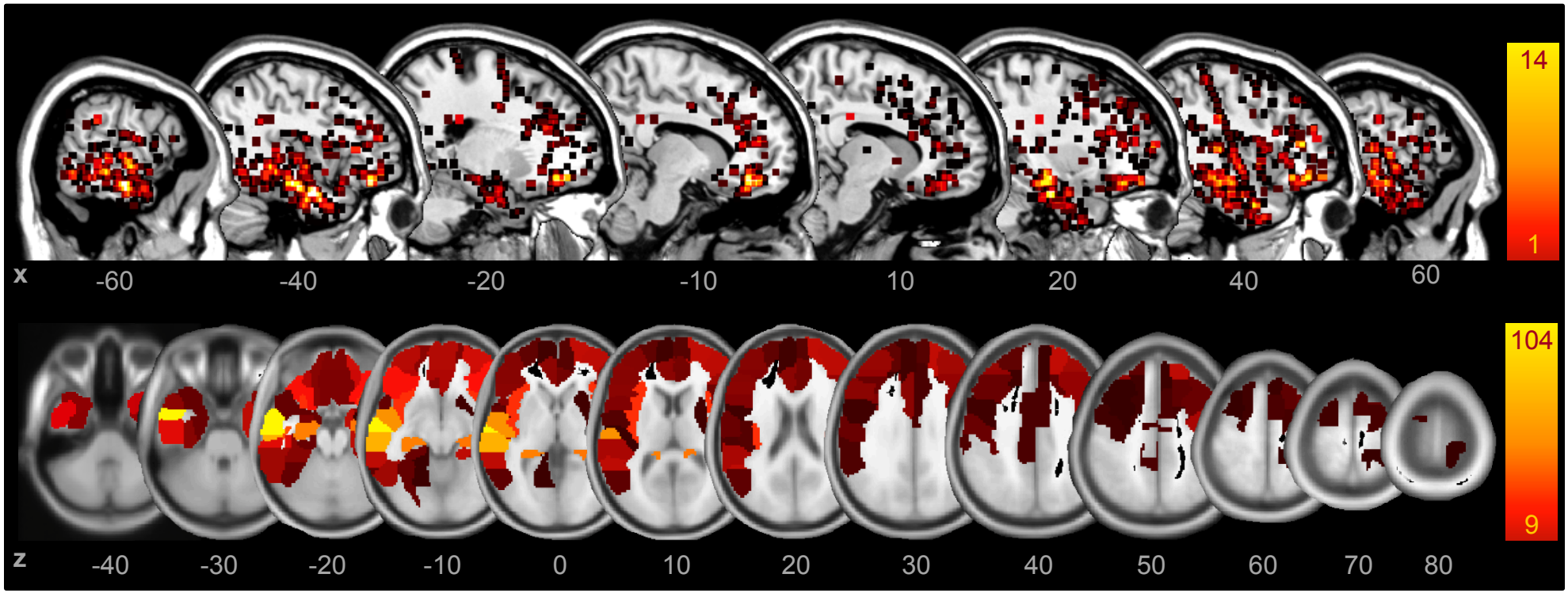
14
1
x
-60
-40
-20
-10
10
20
40
60
104
9
z
-40
-30
-20
-10
0
10
20
30
40
50
60
70
80

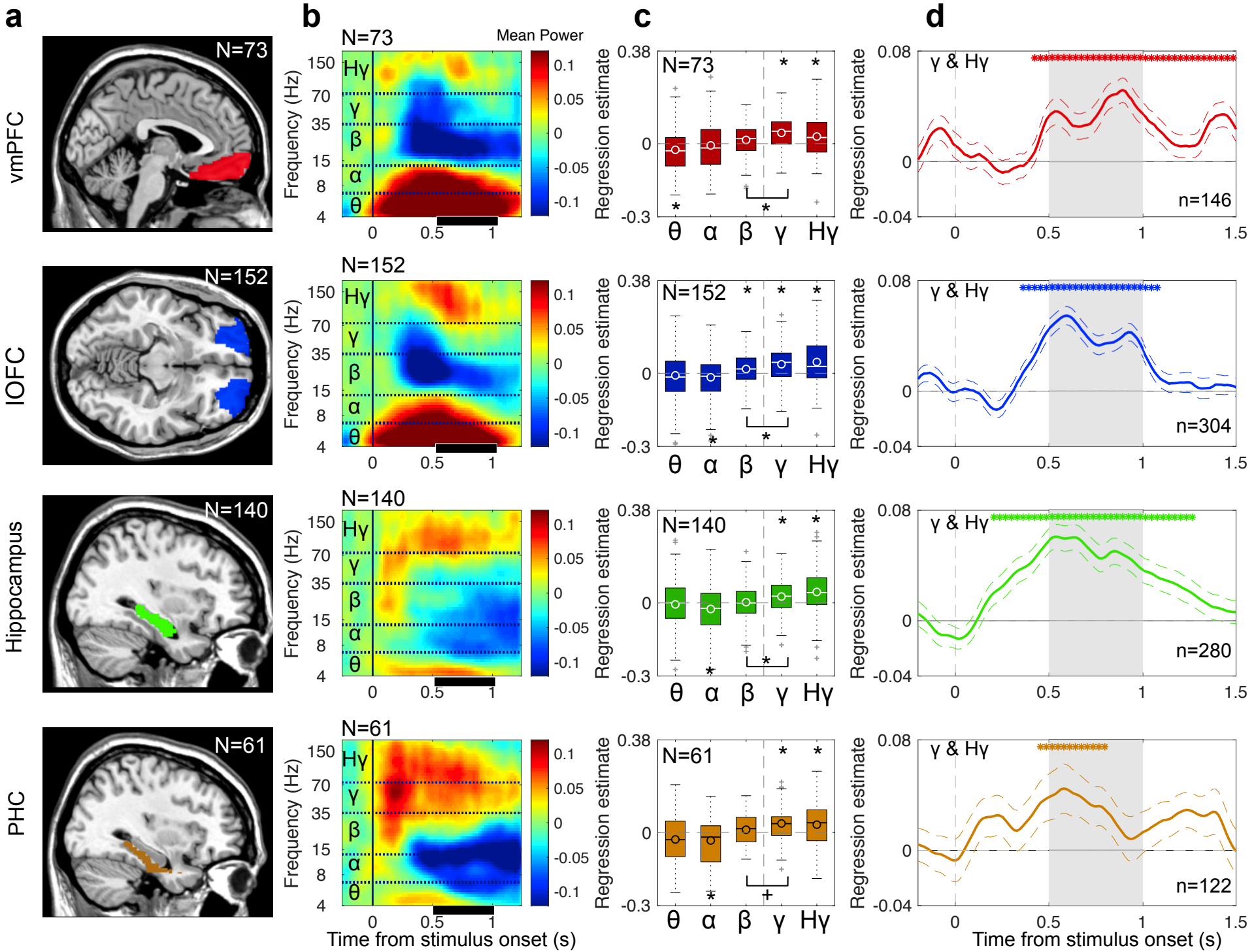
a
b
c
d
vmPFC
lOFC
Hippocampus
PHC
N=73
N=152
N=140
N=61
Mean Power
Frequency (Hz)
Hγ
γ
β
α
θ
Regression estimate
γ & Hγ
n=146
n=304
n=280
n=122
Time from stimulus onset (s)

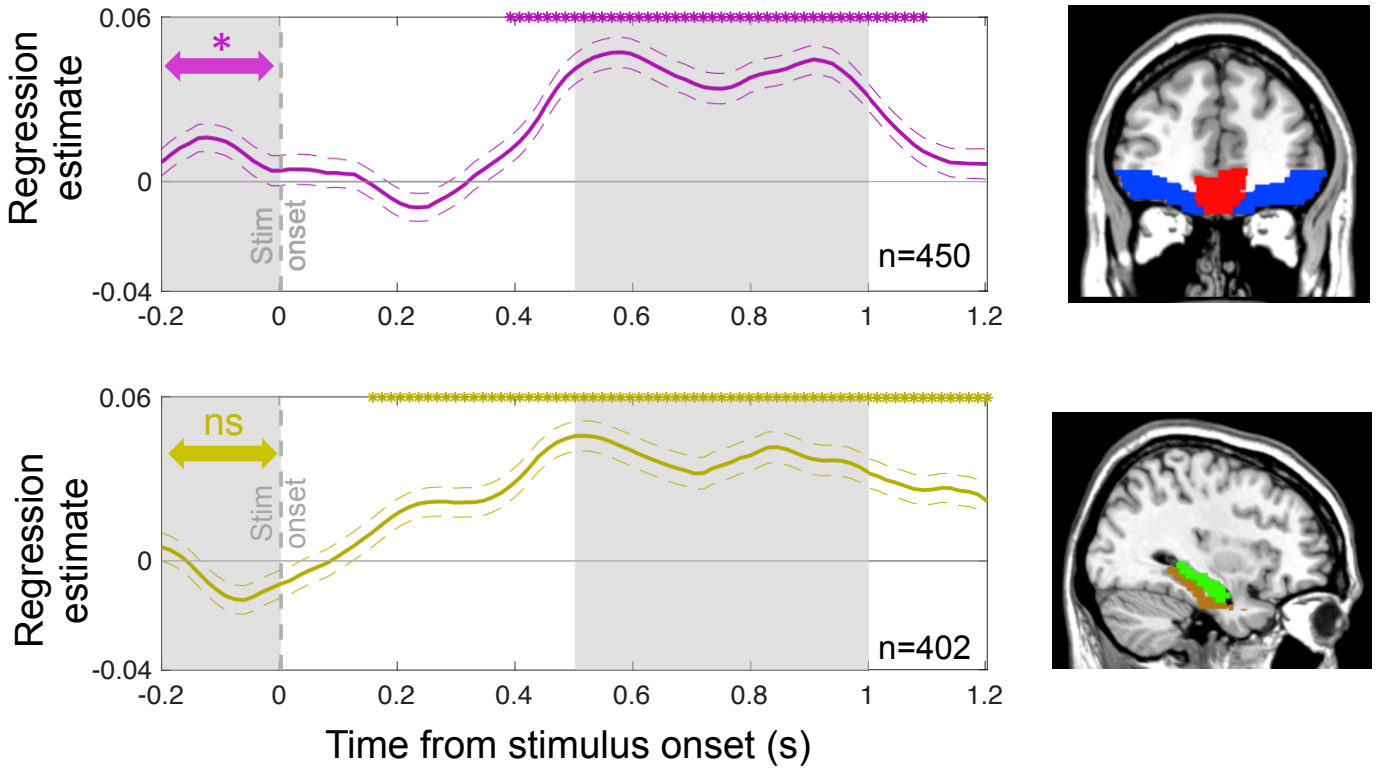
Regression estimate
0.06
0
-0.04
*
Stim onset
n=450
-0.2
0
0.2
0.4
0.6
0.8
1
1.2
ns
n=402
Time from stimulus onset (s)

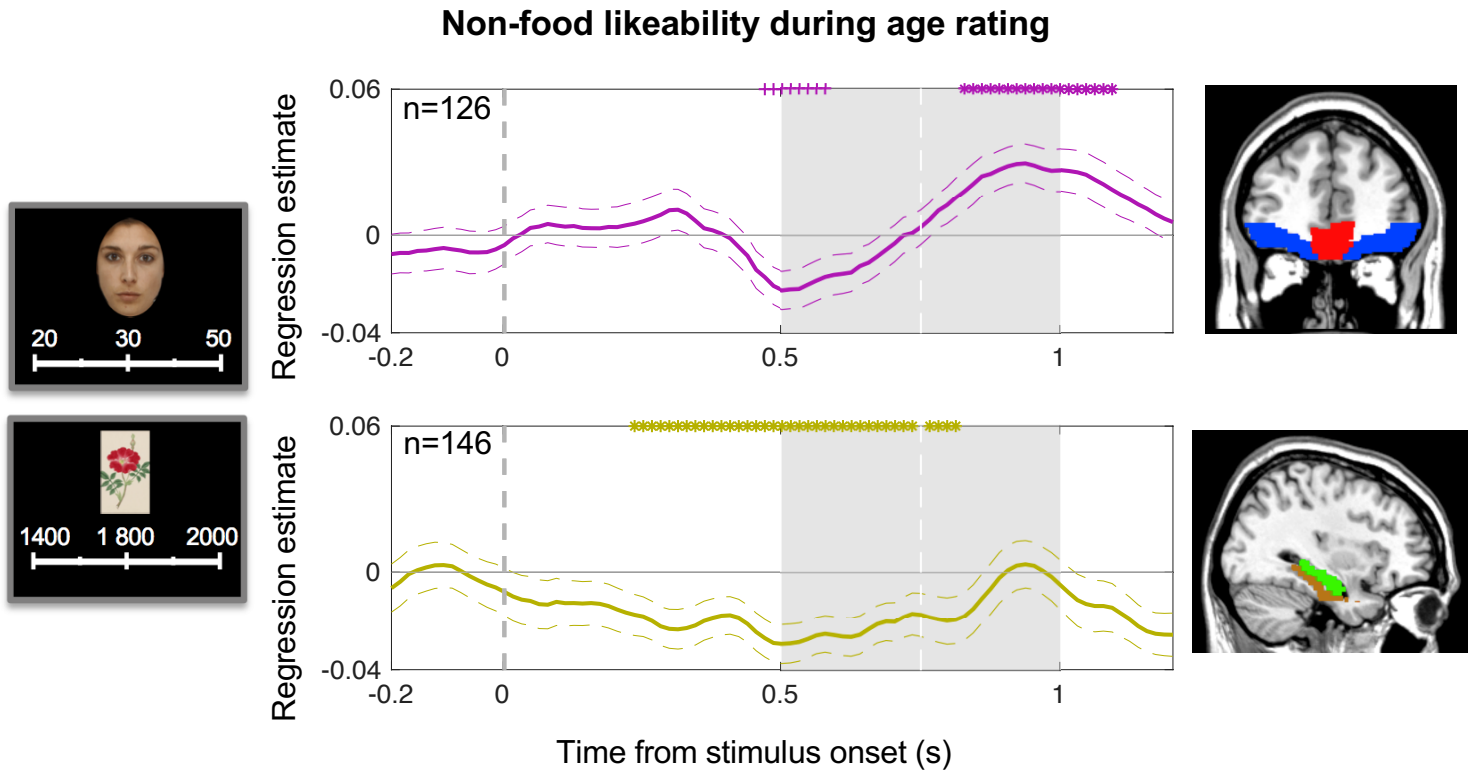
Non-food likeability during age rating
20
30
50
1400
1 800
2000
n=126
n=146
0.06
0
-0.04
-0.2
0
0.5
1
Regression estimate
Time from stimulus onset (s)

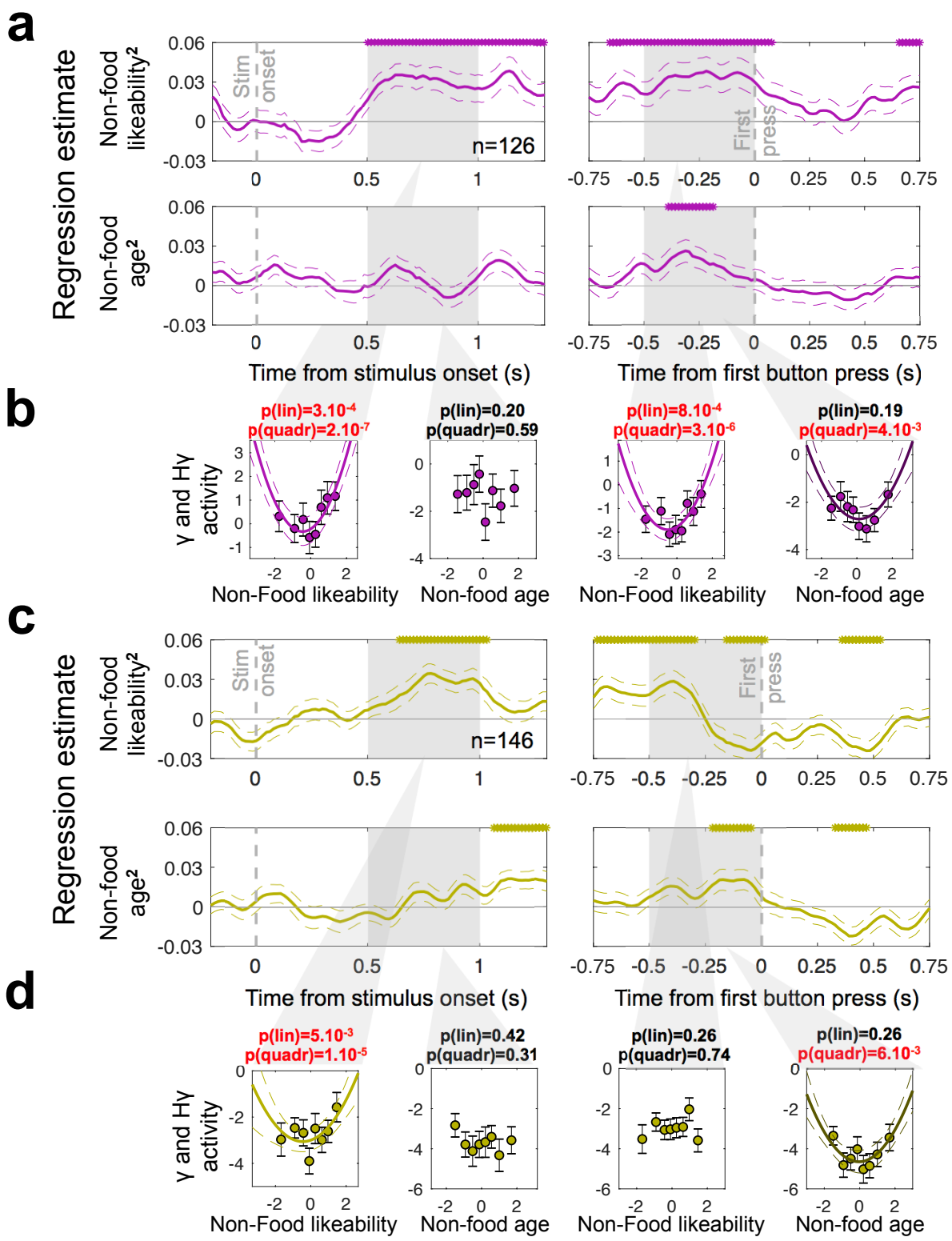
a
Regression estimate
Non-food likeability²
Non-food age²
Stim onset
First press
n=126
Time from stimulus onset (s)
Time from first button press (s)
b
p(lin)=3.10-4
p(quadr)=2.10-7
p(lin)=0.20
p(quadr)=0.59
p(lin)=8.10-4
p(quadr)=3.10-6
p(lin)=0.19
p(quadr)=4.10-3
γ and Hγ activity
Non-Food likeability
Non-food age
c
n=146
d
p(lin)=5.10-3
p(quadr)=1.10-5
p(lin)=0.42
p(quadr)=0.31
p(lin)=0.26
p(quadr)=0.74
p(lin)=0.26
p(quadr)=6.10-3

Supplementary Table 1: Demographical data

Task version	Recording center	ID	Sex	Age (years)	Epilepsy onset (age)	Suspected Epileptic focus	Intellectual Quotient (IQ)	Hand laterality	Number of electrodes	Number of recording sites	Number of sites in vmPFC	Number of sites in lOFC	Number of sites in Hippocampus	Number of sites in PHC
Complete	Grenoble	G1	M	37	29	Left OFC	NA	NA	13	165	9	10	0	0
Short		G2	F	31	24	Left temporal	100	R	12	156	0	0	6	0
Short		G3	M	47	38	Right temporal	96	R	18	328	4	2	11	2
Short		G4	F	34	26	Right OFC	76	R	16	208	2	6	2	2
Short & Complete		G5	F	47	19	Bi-fronto-temporal	120	R	16	203	2	16	2	2
Short (only rating)		G6	M	57	37	Left anterior temporal	104	NA	12	187	5	5	4	4
Complete		G7	F	39	28	Left temporal	76	R	17	229	2	0	1	6
Short	Lyon	L1	F	49	39	Right temporal	NA	R	14	149	1	6	4	4
Short		L2	M	21	14	Left fronto-temporal	NA	R	15	168	2	6	5	0
Short		L3	F	43	2	Left temporale	NA	R	13	129	2	12	4	0
Short		L4	F	40	15	NA	NA	L	11	109	0	0	9	0
Short		L5	F	38	28	Left temporal	NA	R	9	98	0	0	6	0
Short		L6	M	22	NA	NA	NA	L	11	133	6	8	2	4
Short		L7	F	48	19	Right temporal	NA	R	13	149	2	6	2	2
Short		L8	M	41	NA	Left temporal	NA	L	5	50	1	4	1	0
Short		L9	M	30	NA	Right fronto-temporal	NA	R	13	149	5	4	11	0
Short		L10	F	21	4	Left frontal / insula	NA	R	11	115	2	4	0	0
Short		L11	M	26	21	NA	NA	R	12	132	4	4	8	3
Short		L12	F	43	40	Left temporal	NA	L	13	126	3	2	6	0
Short		L13	F	26	4	Left anterior temporal	NA	R	13	127	3	3	1	0
Short		L14	F	31	NA	NA	NA	R	12	121	2	7	0	0
Short		L15	F	45	21	Left temporal /insula	NA	R	10	110	0	0	9	0
Short		L16	M	44	NA	NA	NA	R	11	114	2	1	2	5
Short		L17	M	48	NA	NA	NA	R	14	153	1	5	0	0
Short		L18	M	51	11	NA	NA	R	12	128	2	7	4	1
Complete	Paris	P1	M	22	7	Left temporal	79	R	9	78	0	5	5	2
Complete		P2	F	55	36	Right temporal	96	R	11	94	2	1	6	4
Complete		P3	F	60	32	Right anterior temporal	89	L	8	57	0	0	10	3
Complete		P4	F	30	16	dorso-medial frontal	117	R	10	66	3	0	0	0
Complete		P5	M	29	20	Right posterior temporal	NA		8	60	0	0	3	0
Complete		P6	F	22	8	dorso-medial frontal	NA	R	10	58	0	0	0	0
Complete		P7	F	34	9	Left Insula / Amygdala	110	R	8	68	1	5	1	1
Complete		P8	F	39	23	Left anterior temporal	106	R	7	62	1	3	4	2
Complete (without faces)		P9	M	34	12	Right anterior temporal	NA	R	10	78	0	0	2	5
Complete		P10	M	37	24	Right anterior temporal	NA	R	7	50	2	4	1	1
Complete		P11	F	45	25	Right temporal	NA	R	9	78	0	0	6	6

IQ: Intellectual Quotient; NA: Missing Data, OFC: Orbito-Frontal Cortex; R: Right, L: Left, Bi: Bilateral; M: Male; F: Female

Supplementary Table 2: Brain regions obtained from re-parcellation of the AAL atlas

AAL (restructured) label	N	AAL (restructured) label	N	AAL (restructured) label	N
Temporal Mid L ant/ant	148	Frontal Mid L ant/inf	31	Angular L	8
Temporal Mid L ant/post	119	Frontal Inf Oper L	31	Thalamus R	8
Temporal Sup R ant	117	Frontal Sup Orb R	**30**	Occipital Mid R sup	8
Temporal Sup L ant	111	Amygdala L	30	Temporal Mid R post/post	7
Hippocampus L	104	Rectus	**29**	Postcentral R inf/ant	7
Hippocampus R	102	Rolandic Oper R	26	Putamen L	7
Temporal Inf R ant	92	Cingulum Ant R	26	Parietal Inf R	7
Temporal Mid R ant/ant	84	SupraMarginal R	25	Angular R	6
Insula L	82	Frontal Inf Tri R post	25	Cingulum Mid R post	6
Insula R	82	Frontal Mid L post/inf	24	Postcentral R inf/post	6
Temporal Mid R ant/post	80	ParaHippocampal L	23	Parietal Inf L post	5
Frontal Inf Orb R	75	Frontal Mid R post/sup	23	Supp Motor Area R post	4
Frontal Inf Orb L	65	Heschl R	23	Cingulum Post	4
Temporal Inf L ant	57	Postcentral L inf	23	Cuneus R	4
Frontal Mid Orb R	**53**	Temporal Pole Sup L	22	Precuneus R inf	3
Temporal Sup R post	51	Fusiform L post	22	Frontal Sup Medial L sup	3
Temporal Pole Mid R	51	Frontal Sup R post/ant	21	Lingual R ant	3
ParaHippocampal R	49	Frontal Sup L ant	21	Parietal Sup L ant	3
Frontal Sup R ant	49	Temporal Mid L post/post	21	Precentral R sup	3
Temporal Mid L post/ant	48	Temporal Mid R post/ant	18	Precentral L sup	3
Frontal Mid R ant inf	47	Rolandic Oper L	18	Olfactory	2
Frontal Mid Orb L	**45**	Frontal Sup Medial R inf	17	Caudate	2
Frontal Med Orb	**44**	SupraMarginal L	16	Cerebelum L	2
Precentral R inf	43	Cingulum Mid R ant	15	Calcarine R	2
Temporal Sup L post	42	Cingulum Mid L	15	Pallidum R	2
Temporal Inf L post	40	Supp Motor Area R ant	14	Cuneus L	2
Frontal Mid R ant/sup	40	Temporal Inf R post	14	Occipital Sup L	2
Frontal Inf Tri R ant	39	Frontal Sup R post/post	13	Caudate R	2
Frontal Mid L ant/sup	37	Frontal Sup Medial L inf	12	Fusiform R post	2
Frontal Mid R post/inf	37	Frontal Sup L post	12	Paracentral Lobule	2
Fusiform R ant	36	Putamen R	12	Parietal Sup R ant	2
Frontal Inf Oper R	35	Precentral L inf	12	Precuneus L inf	2
Temporal Pole Mid L	34	Frontal Sup Medial R sup	10	Occipital Inf L	1
Frontal Inf Tri L post	34	Lingual L ant	10	Supp Motor Area L ant	1
Cingulum Ant L	34	Heschl L	10	Pallidum L	1
Fusiform L ant	33	Amygdala R	9	Occipital Sup R	1
Temporal Pole Sup R	33	Frontal Mid L post/sup	9	Occipital Mid L ant	1
Frontal Inf Tri L ant	33	Postcentral R sup	9	Precuneus L sup	1
Frontal Sup Orb L	**32**			NA	235

Inf: inferior; Sup: Superior; Ant: Anterior; Post: Posterior; L: Left; R: Right; Mid: Middle; Med: Median; Tri: Triangularis; Supp: Supplementary; Orb: Orbital; Oper: Opercular.; NA: Not Attributed. Grey: Areas not included in the pseudo whole-brain analysis (less than 9 recorded sites). Red: vmPFC; blue: lOFC; green: hippocampus; orange: PHC. N indicates the number of recording sites.

Supplementary Table 3: Pseudo whole-brain analysis of food value signaling in a priori high-gamma range (50-150Hz)

POSITIVE CORRELATION WITH VALUE				
AAL label	**Number of sites**	**Significant sites (%)**	**max t-value**	**p-value**
Hippocampus L	104	36	291,54	$< 5.10^{-4}$ *
Hippocampus R	102	40	245,32	$< 5.10^{-4}$ *
Frontal Mid Orb L	45	44	133,16	$< 5.10^{-4}$ *
Frontal Sup R ant	49	34	129,83	$< 5.10^{-4}$ *
Temporal Inf L ant	57	28	114,25	$< 5.10^{-4}$ *
Frontal Mid R ant/inf	47	24	110,39	$< 5.10^{-4}$ *
ParaHippocampal L	23	47	107,39	$< 5.10^{-4}$ *
Frontal Sup Orb R	30	37	107,29	$< 5.10^{-4}$ *
Fusiform L ant	33	39	97,33	$< 5.10^{-4}$ *
Fusiform R ant	36	44	79,98	5.10^{-4} *
Frontal Mid Orb R	53	34	77,49	$< 5.10^{-4}$ *
Frontal Med Orb	44	36	77,18	$< 5.10^{-4}$ *
Frontal Inf Tri L ant	33	36	76,97	$< 5.10^{-4}$ *
Frontal Mid L post/sup	9	44	75,1	5.10^{-4} *
ParaHippocampal R	49	27	69,13	$< 5.10^{-4}$ *
Fusiform L post	22	41	62,63	5.10^{-4} *
Frontal Sup Orb L	32	41	60,05	$< 5.10^{-4}$ *
Temporal Pole Sup R	33	39	50,58	2.10^{-3}
Precentral L inf	12	50	49,63	6.10^{-3}
SupraMarginal R	25	44	49,44	5.10^{-4} *
Cingulum Ant L	34	24	43,29	3.10^{-3}
Frontal Inf Oper R	35	26	39,18	4.10^{-3}
Frontal Sup Medial L inf	12	25	37,76	8.10^{-3}
Rectus	29	28	33,35	4.10^{-3}
Temporal Pole Mid L	34	26	31,29	6.10^{-3}
Temporal Mid L ant/ant	148	24	31,14	8.10^{-3}
Temporal Mid R ant/post	80	28	30,71	8.10^{-3}
Cingulum Ant R	26	23	30,38	8.10^{-3}
Temporal Inf R ant	92	27	30,2	8.10^{-3}
Frontal Inf Tri R post	25	24	29,74	9.10^{-3}
Temporal Inf L post	40	25	27,3	0,01
Temporal Mid R post/ant	18	33	25,12	0,02
Cingulum Mid L	15	33	21,33	0,02
Frontal Inf Oper L	31	26	13,95	0,04
Insula L	82	23	13,26	0,049

NEGATIVE CORRELATION WITH VALUE			
AAL label	**Number of sites**	**max t-value**	**p-value**
Heschl R	23	-159,21	$< 5.10^{-4}$ *
Heschl L	10	-124,58	$< 5.10^{-4}$ *
Postcentral R sup	9	-107,97	$< 5.10^{-4}$ *
Temporal Sup R ant	117	-103,31	$< 5.10^{-4}$ *
Frontal Mid R post sup	23	-81,31	$< 5.10^{-4}$ *
Precentral R inf	43	-62,37	5.10^{-4} *
Temporal Sup L ant	111	-59,21	5.10^{-4} *
Frontal Mid L ant inf	31	-39,33	0.0025*
Amygdala R	9	-27,91	0,014
Temporal Sup R post	51	-24,38	0,017
Frontal Mid R post inf	37	-23,47	0,0135
Cingulum Mid R ant	15	-22,1	0,027
Frontal Inf Tri R ant	39	-20,53	0,024

Same abbreviations as in Supplementary Table 2. Areas are ordered according to the maximal t-value obtained at cluster level in the regression of high-gamma activity against food likeability rating. Red: vmPFC; blue: lOFC; green: hippocampus; orange: PHC, grey: significant bilateral regions included in the extended BVS. p-values are obtained with two-sided one-sample t-tests cluster-wise corrected ($p<0.05$). Stars indicate significance after Bonferroni-Holm correction for multiple comparisons across regions.

Supplementary Table 4: Pseudo whole-brain analysis of food value signaling in a priori gamma range (35-50Hz)

POSITIVE CORRELATION WITH VALUE			
AAL label	**Number of sites**	**max t-value**	**p-value**
Frontal Inf Tri L post	34	87,75	$< 5.10^{-4}$ *
Frontal Inf Orb L	65	80,43	$< 5.10^{-4}$ *
Frontal Med Orb	42	61,51	0.001*
Frontal Sup R ant	49	54,97	0.0005*
Frontal Inf Oper R	35	53,76	0.0015*
Frontal Inf Tri L ant	33	43,63	0.003*
Frontal Mid Orb L	45	34,99	0,015
Temporal Sup R post	45	33,36	0,018
Frontal Mid L ant/inf	31	33,08	0,0155
Cingulum Ant L	34	32,91	0,016
Rolandic Oper L	18	31,42	0,022
Frontal Mid L post/sup	9	30,78	0,039
Frontal Mid Orb R	53	25,02	0,048

NEGATIVE CORRELATION WITH VALUE			
AAL label	**Number of sites**	**max t-value**	**p-value**
Postcentral L inf	23	-43,61	0.004*
Rolandic Oper R	21	-42,06	0.009*
Frontal Mid R post/inf	36	-35,05	0.0135*
Frontal Inf Tri R ant	39	-34,11	0.017*

Same legend as in Supplementary Table 3. Areas are ordered according to the maximal t-value obtained at cluster level in the regression of gamma activity against food likeability rating. p-values are obtained with two-sided one-sample t-tests cluster-wise corrected ($p<0.05$).

Supplementary Table 5: Pseudo whole-brain analysis of food value signaling in a priori beta range (15-35Hz)

POSITIVE CORRELATION WITH VALUE			
AAL label	**Number of sites**	**max t-value**	**p-value**
Frontal Sup Medial R sup	10	67,66	0.001*
Temporal Sup L ant	111	63,69	0.001*
Temporal Sup L post	42	55,01	0.0025*
Temporal Mid R ant/ant	84	54,08	0.0045*
Frontal Sup R post/ant	21	52,94	0.0045*
Frontal Mid R ant/sup	40	46,76	0,007
Frontal Sup Orb L	32	41,41	0,013
Temporal Mid R ant/post	80	39,55	0,017
Hippocampus R	102	34,99	0,0215
Frontal Mid Orb R	53	33,79	0,0155
Frontal Inf Tri L post	34	33,01	0,029
Frontal Sup R post/post	13	32,85	0,035
Frontal Mid Orb L	45	27,61	0,048
Temporal Mid L ant/ant	148	27,05	0,0455

NEGATIVE CORRELATION WITH VALUE			
AAL label	**Number of sites**	**max t-value**	**p-value**
Temporal Mid L post/post	21	-140,8	$< 5.10^{-4}$ *
Temporal Mid L ant/post	119	-107,3	$< 5.10^{-4}$ *
Precentral L inf	12	-91,45	$< 5.10^{-4}$ *
Temporal Mid L post/ant	48	-86,63	$< 5.10^{-4}$ *
Temporal Inf L post	40	-72,3	$< 5.10^{-4}$ *
Cingulum Mid L	15	-63,37	0.001*
Temporal Sup R post	51	-54,2	0.0035*
Precentral R inf	43	-53,04	0.0035*
SupraMarginal L	16	-40,79	0,026
Temporal Sup R ant	117	-36,38	0,0205
Frontal Mid L post/sup	9	-35,89	0,032
Temporal Pole Mid R	51	-35,6	0,034
Amygdala R	9	-35,18	0,043
Frontal Mid R post/sup	23	-33,39	0,0255
Postcentral L inf	23	-30,97	0,035
Frontal Inf Tri R ant	39	-29,65	0,0325

Same legend as in Supplementary Table 3. Areas are ordered according to the maximal t-value obtained at cluster level in the regression of beta activity against food likeability rating. p-values are obtained with two-sided one-sample t-tests cluster-wise corrected ($p<0.05$).

Supplementary Table 6: Pseudo whole-brain analysis of food value signaling in a priori alpha range (8-15Hz)

POSITIVE CORRELATION WITH VALUE			
AAL label	**Number of sites**	**max t-value**	**p-value**
Frontal Sup Medial R sup	10	335,35	$< 5.10^{-4}$ *
Temporal Sup L post	42	274,59	$< 5.10^{-4}$ *
Temporal Sup L ant	111	193,29	5.10^{-4} *
Frontal Sup R post/post	13	184,74	0.001*
Supp Motor Area R ant	14	90,21	0,024
Frontal Sup R ant	49	86,1	0,019
Rolandic Oper R	21	77,15	0,029

NEGATIVE CORRELATION WITH VALUE			
AAL label	**Number of sites**	**max t-value**	**p-value**
Frontal Mid L post inf	24	-275,05	$< 5.10^{-4}$ *
Frontal Sup L post	12	-255,51	$< 5.10^{-4}$ *
Temporal Mid L post/ant	48	-209,09	$< 5.10^{-4}$ *
Temporal Pole Mid L	34	-166,33	$< 5.10^{-4}$ *
Frontal Inf Tri R post	25	-159,54	0.0035*
Temporal Inf L post	40	-153,7	5.10^{-4} *
Hippocampus R	82	-153,63	0.0025*
Frontal Inf Tri L post	34	-146,89	0.0015*
Cingulum Mid L	15	-126,21	0,007
Temporal Pole Mid R	45	-124,75	0,007
Temporal Mid L post/post	21	-122,76	0,013
Frontal Mid L ant inf	31	-114,33	0,006
Frontal Mid L post sup	9	-112,01	0,013
Fusiform L post	22	-108,37	0,007
Temporal Mid L ant/post	119	-97,21	0,015
Frontal Sup Orb R	29	-79,55	0,029
Temporal Sup R post	45	-78,93	0,029
Precentral R inf	43	-75,22	0,043
Hippocampus L	105	-73,99	0,025
SupraMarginal L	16	-67,09	0,039

Same legend as in Supplementary Table 3. Areas are ordered according to the maximal t-value obtained at cluster level in the regression of alpha activity against food likeability rating. p-values are obtained with two-sided one-sample t-tests cluster-wise corrected ($p<0.05$).

Supplementary Table 7: Pseudo whole-brain analysis of food value signaling in a priori theta range (4-7Hz)

POSITIVE CORRELATION WITH VALUE			
AAL label	**Number of sites**	**max t-value**	**p-value**
Temporal sup L post	42	227,21	$< 5.10^{-4}$ *
Frontal sup R post/ant	21	198,77	0.001*
Temporal inf R post	14	121,89	0.003*
Frontal sup Medial R sup	10	108,07	0,015
Putamen R	12	73,73	0,045
Frontal Mid R ant sup	40	72,86	0,031
Cingulum Mid L	15	62,95	0,042
Temporal Pole sup L	22	62,01	0,047

NEGATIVE CORRELATION WITH VALUE			
AAL label	**Number of sites**	**max t-value**	**p-value**
Frontal Mid L post inf	24	-297,66	< 5.10-4 *
Frontal sup L post	12	-292,35	< 5.10-4 *
Frontal inf Tri R post	25	-240,08	< 5.10-4 *
Frontal inf Oper L	31	-229,31	5.10-4 *
Frontal inf Tri L ant	33	-189,11	5.10-4 *
Frontal Mid Orb L	45	-169,32	0.001*
Temporal Mid R ant/post	68	-152,1	0.001*
Frontal Mid L ant inf	31	-127,85	0,004
supraMarginal L	16	-127,16	0,003
Temporal Mid L post/ant	48	-125,47	0,004
Precentral L inf	12	-120,72	0,007
Frontal inf Tri R ant	39	-116,39	0,007
postcentral L inf	23	-115,26	0,007
Temporal Pole Mid L	34	-114,85	0,006
Temporal Mid L ant/ant	148	-110,47	0,011
Frontal Mid Orb R	53	-105,93	0,013
Precentral R inf	43	-103,15	0,012
Frontal inf Orb L	65	-94,21	0,019
Temporal sup R post	45	-87,12	0,015
Rectus combined	29	-85,67	0,022
Fusiform R ant	34	-78,73	0,026
Frontal inf Tri L post	34	-78,63	0,02
Frontal Mid R ant inf	47	-78,48	0,026
Temporal sup R ant	95	-76,23	0,025
Frontal inf Orb R	68	-66,9	0,04
Temporal inf R ant	79	-65,44	0,035
ParaHippocampal L	23	-60,59	0,047

Same legend as in Supplementary Table 3. Areas are ordered according to the maximal t-value obtained at cluster level in the regression of theta activity against food likeability rating. p-values are obtained with two-sided one-sample t-tests cluster-wise corrected ($p<0.05$).

Supplementary Table 8: Functional properties in the supplementary BVS areas

		ANTICIPATION	GENERICITY	AUTOMATICITY		QUADRATICITY
				0.5 – 0.75s	0.75 – 1s	
Temporal inferior	n	298	126	126	126	298
	mean	-0,006	-0,022	-0,001	0,009	0,019
	SEM	*0,004*	*0,006*	*0,009*	*0,008*	*0,005*
	df	297	127	127	127	297
	t	-1,267	-3,362	-0,088	1,11	4,064
	p	0,206	**0,001**	0,93	0,269	**6.10^{-5}**
Fusiform anterior	n	88	64	64	64	88
	mean	0,008	-0,007	-0,027	-0,003	0,028
	SEM	*0,009*	*0,009*	*0,011*	*0,01*	*0,008*
	df	87	65	65	65	87
	t	0,976	-0,771	-2,448	-0,342	3,45
	p	0,332	0,443	**0,017**	0,733	**0,001**
Cingulate	n	94	14	14	14	94
	mean	0,004	0,02	-0,001	-0,011	0,016
	SEM	*0,007*	*0,011*	*0,019*	*0,017*	*0,008*
	df	93	15	15	15	93
	t	0,586	1,815	-0,061	-0,644	2,011
	p	0,56	0,09	0,952	0,529	**0,047**
Frontal inferior opercularis	n	66	38	38	38	66
	mean	0,001	0,017	-0,029	-0,008	-0,036
	SEM	*0,011*	*0,014*	*0,017*	*0,013*	*0,012*
	df	65	39	39	39	65
	t	0,08	1,22	-1,771	-0,581	-3,062
	p	0,937	0,23	0,084	0,565	**0,003**

Summary statistics for each functional property in the supplementary BVS regions (two-sided one-sample Student's test). Abreviations: SEM: Standard error of the mean; df: degree of freedom; t: t-value; p: p-value; n: number of power time series included in the analysis. In bold are the significant results. Anticipation: test of the food likeability regression estimates on the -0.2-0s time window before stimulus onset. Genericity: test of the non-food likeability regression estimates on the 0.5-1.0s time window after stimulus onset. Automaticity: test of the non-food likeability regression estimates during the age-rating task on the 0.5-0.75s and 0.75-1.0s time windows after stimulus onset. Quadraticity: test of the food likeability squared rating regression estimates during the food likeability rating task on the -0.5-0s time window before response onset.

Four core properties of the human brain valuation system demonstrated in intracranial signals

Supplementary information

Supplementary Figure 1 – Temporal dependencies of value signals across brain regions

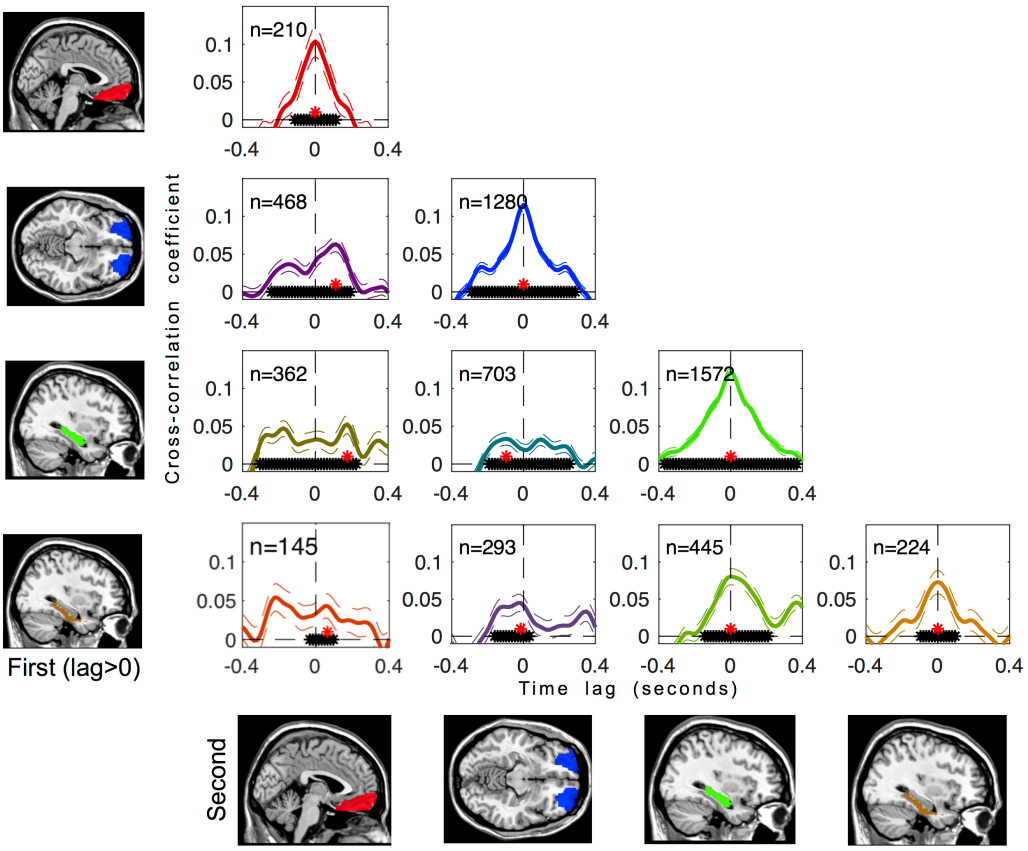

To better specify the propagation of value signals across time during food likeability rating trials, we conducted a cross-correlation analysis between the high-gamma regression estimates of all possible within-subject pairs of recording sites in BVS regions.

Plots show pairwise Pearson's correlation coefficient of regression estimates (food likeability rating regressed against high-gamma activity) between regions of interest, calculated across trials for every time point. Black stars indicate significant correlations (two-sided one-sample t-test, $p<0.05$, cluster corrected), red stars point to the peaks of significant correlations. n is the number of within-subject pairs of recording sites included in the correlation analysis. Regions: vmPFC (red), lOFC (blue); hippocampus (green); PHC (brown). The color of cross-correlograms is a mixture of the two colors of correlated brain regions (e.g., purple for vmPFC and lOFC). Solid (and dashed) lines indicates mean (and SEM) across n pairs of recording sites.

This analysis revealed that all pairs were significantly correlated, with variable time-lags. First, the pairs located within each ROI showed significant correlation with a mean

time-lag of zero, suggesting that value signals emerged at about the same time across the contacts situated in a same BVS region. Second, vmPFC value signals appeared later (mean lag of 112ms) than lOFC signals. Third, there was no significant time-lag between hippocampus and PHC regions, which were thus signaling value simultaneously. The time-lags between OFC and (P)HC regions must be taken with caution, as there was no clear correlation peak. The presence of correlation peaks at both negative and positive time-lags could reflect a two-way exchange of value-related information between ROIs.

Supplementary Figure 2 – Temporal dependencies of value signals across brain regions in the extended BVS

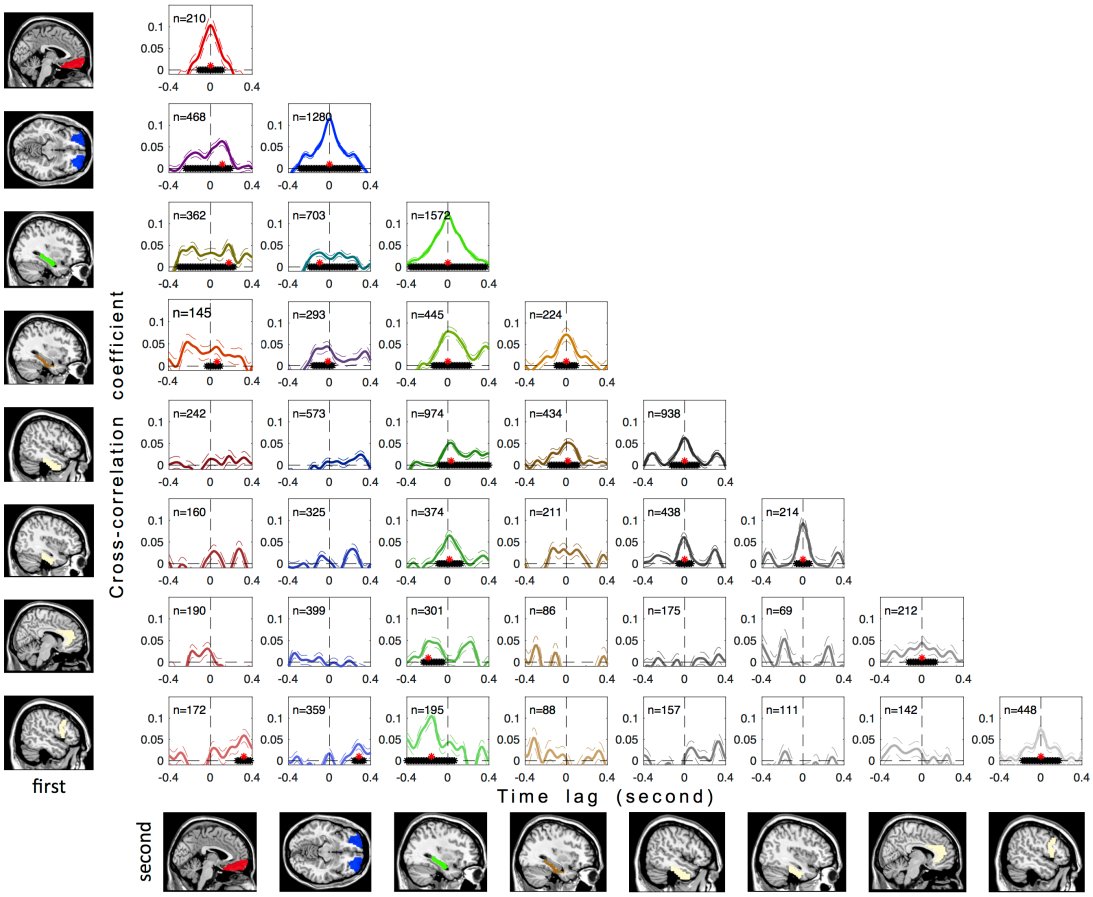

The analysis is identical to that illustrated in the previous figure, but it now includes every region of the extended BVS.
Plots show pairwise Pearson's correlation coefficients of regression estimates (food likeability rating regressed against high-gamma activity) between regions of interest, calculated across trial for every time point. Positive time lag indicates that the region in rows (first) preceeds the region in columns (second). Black stars indicate significant correlations (two-sided one-sample t-test, $p<0.05$, cluster corrected), red stars point to the peaks of significant correlations. n is the number of within-subject pairs of recording sites included in the correlation analysis. Regions of the BVS: vmPFC (red), lOFC (blue); hippocampus (green); PHC (brown). The color of cross-correlograms is a mixture of the two colors of correlated brain regions (e.g., purple for vmPFC and

lOFC). Regions of the extended BVS are shown in yellow (from left to right, and top to bottom: inferior temporal cortex, fusiform anterior gyrus, anterior cingulate gyrus and opercular part of the inferior frontal gyrus). Solid (dashed) lines indicates mean (SEM) across pairs of recording sites.